This document is the accepted manuscript version of the following article:

Yang, S. Y., Yan, Y., Lothenbach, B., & Skibsted, J. (2021). Incorporation of sodium and aluminum in cementitious calcium-alumino-silicate-hydrate C-(A)-S-H phases studied by 23Na, 27Al, and 29Si MAS NMR spectroscopy. Journal of Physical Chemistry C, 125(51), 27975-27995. https://doi.org/10.1021/acs.jpcc.1c08419

Incorporation of Sodium and Aluminum in Cementitious Calcium-Alumino-Silicate-Hydrate C-(A)-S-H Phases Studied by ^{23}Na, ^{27}Al and ^{29}Si MAS NMR Spectroscopy

Sheng-Yu Yang[1], Yiru Yan[2], Barbara Lothenbach[2], Jørgen Skibsted[1]*

[1] Department of Chemistry and Interdisciplinary Nanoscience Center (*i*NANO), Aarhus University, DK-8000 Aarhus C, Denmark

[2] Concrete & Asphalt Laboratory, Empa, 8600 Dübendorf, Switzerland

* Corresponding author: Jørgen Skibsted, Department of Chemistry and Interdisciplinary Center (*i*NANO), Aarhus University, Langelandsgade 140, DK-8000 Aarhus C. Tel.: +45 2899 2029; E-mail address: jskib@chem.au.dk

Abstract

The partial replacement of Portland cement by aluminosilicate-rich supplementary cementitious materials (SCMs) represents a valuable approach to lower the CO_2 footprint of concrete. However, SCMs alter the composition and structure of the principal binding component, C-(A)-S-H, a less-crystalline aluminum-substituted calcium silicate hydrate. The uptake and structural impact of alkalis and aluminum is investigated for synthesized C-(A)-S-H phases with different Ca/Si and Al/Si ratios and alkali (Na^+) contents, using solid-state ^{23}Na, ^{27}Al and ^{29}Si NMR as principal analytical tools. $^{29}Si\{^1H\}$ CP/MAS NMR data propose that the -87 ppm resonance originates from a second type of Q^2 pairing sites most likely in the middle of octameric or longer silicate units. This assignment along with constraints induced by the silicate dreierketten structure results in reliable simulations of the ^{29}Si NMR spectra. A quantitative 1:1 relation between the Al/Si ratios from ^{29}Si NMR and the content of four-fold coordinated Al from ^{27}Al NMR is observed, which reveals that the ^{29}Si $Q_p^2(1Al)$ resonance is only associated with Al(IV) in C-(A)-S-H. Combined analysis of the ^{27}Al and ^{29}Si NMR spectra can account for six-fold coordinated Al being present in the bridging sites of the silicate chains as proposed very recently. The sodium uptake is found to decrease with increasing Ca/Si ratio. For C-(A)-S-H phases with high Ca/Si ratios (Ca/Si $\gtrsim$ 1.0), sodium promotes the incorporation of Al(IV) in the silicate chains, but not at low Ca/Si ratios (Ca/Si $\lesssim$ 1.0). The results indicate that the mutual uptake of alkali and Al ions is governed by more than one mechanism and depends on the composition/structure of the C-(A)-S-H phase.

INTRODUCTION

Portland cement is the most widely used construction material in the world with an annual production surpassing four billion tons in recent years.[1] As a result of this massive consumption, Portland cement production is responsible for 6 - 7% of the anthropogenic CO_2 emissions,[1,2] which mainly originate from the decomposition of limestone ($CaCO_3$) and from fossil fuel combustion to generate thermal energy. Thus, reduction of the CO_2 footprint from cement production represents a highly important industrial research challenge, also considering that cement production is forecasted to significantly increase over the next 30 years.[1,3] The addition of supplementary cementitious materials (SCMs), such as fly ashes, slags and calcined clays to cement represents a valuable and widely adopted approach to efficiently reduce the amount of Portland cement clinker in concrete and thereby the 'materials' CO_2 footprint of cement production.[4] The most commonly used SCMs comprise high contents of aluminium and silicon, which by their pozzolanic reaction will modify the composition and hydrate phase assemblages of the hydrated composite cements.[5,6] This includes the composition and microstructure of the calcium-silicate-hydrate (C-S-H) phase, which is the principal component in hardened cement responsible for strength development. Significant reductions in CO_2 emission may also be achieved for alternative binders such as 'geopolymers', which are based on alkali-activation of waste products such as slags and fly ashes or other alumino-silicate rich phases.[7,8] The reduction in CO_2 emission for these materials is mainly related to their low calcium content, however, these types of binders still await a breakthrough on a larger industrial scale.

The C-S-H phase and its Al substituted analogue, C-(A)-S-H: $(CaO)_x(Al_2O_3)_ySiO_2(H_2O)_z$, exhibits a less-ordered/amorphous structure which composition depends on the hydrating medium it is formed in, and thereby on the presence of SCMs. The C-(A)-S-H phase can have Ca/Si ratios in the range 0.6 – 2.0 and Al/Si ratios up to approx. 0.2 with a basic structure that can be described by the defect tobermorite model.[9-12] Tobermorite has a layered structure consisting of CaO_2 layers, with seven-fold coordinated Ca^{2+} ions, where the oxygens are shared with 'dreierketten' chains of SiO_4 tetrahedra on both sides of the CaO_2 layer, including bridging and paired SiO_4 tetrahedra.[13] Water molecules and additional Ca^{2+} ions are present in between these layers which are separated by 11 – 15 Å. The variation in Ca/Si ratio can be accounted for by removal of Si atoms from the bridging sites of the silicate chains and by incorporation of additional Ca^{2+} ions in the interlayer.[12,14]

Aluminium is preferentially incorporated in the C-S-H structure by substitution for the four-fold coordinated Si atoms in the bridging sites of the silicate chains, Al(IV), as evidenced from experimental ^{27}Al and ^{29}Si NMR studies[15-18] and atomistic simulations.[19,20] In addition, an appreciable

amount of aluminium can also be present in five-fold (Al(V)) and octahedral ((Al(VI)) coordination, where the five-fold coordinated aluminate units are present in the interlayer of the C-(A)-S-H structure, probably replacing interlayer Ca^{2+} sites.[17,21] It has also been proposed that octahedrally coordinated Al is present in the interlayer of the C-(A)-S-H structure,[17,22-24] accounting for the increased basal spacing with increasing Al(VI) content, or at the surface of the C-(A)-S-H particles as a precipitate,[21,22] considering the thermally unstable properties of the hydroxylated AlO_6 species. Most recently, atomistic simulations have suggested that the Al(V) and Al(VI) sites are aluminate species located in the bridging sites of the silicate structure for C-(A)-S-H phases with high Ca/Si ratios.[25]

The quantity of Al incorporated in the C-S-H phase depends on the dissolved aluminium, calcium, silicon and hydroxide (pH) concentrations in the pore solution of the hydrating cements or in the aqueous solution for synthesized C-(A)-S-H samples. The uptake of Al increases with the aqueous aluminium concentration[26,27] and thereby with increasing pH, which promotes the dissolution of aluminate species. However, high aluminium concentrations may also lead to the formation of secondary phases such as katoite ($Ca_3Al_2(OH)_{12}$), strätlingite ($(CaO)_2Al_2O_3SiO_2(H_2O)_8$), alumina gel ($Al(OH)_3$) and other calcium aluminate hydrate (AFm) phases, which for synthesized, equilibrated C-(A)-S-H samples limit the Al/Si ratio to approx. 0.15 independent of the Ca/Si ratio.[28] The Ca/Si ratio of C-(A)-S-H will reflect the calcium and silicon solution concentrations,[28-30] and it has been observed that Al(IV), incorporated in the bridging sites of the silicate tetrahedra, dominates at low Ca/Si ratios whereas high Ca/Si ratios (approx. above 1.2) result in larger fractions of Al(V) and Al(VI) species associated with the C-(A)-S-H structure.[21,23,25,28]

Alkali ions are present in the pore solution of hydrating cements and are often included in C-S-H and C-(A)-S-H syntheses to increase pH and thereby the solubility of aluminate species.[31] In addition, alkali ions may also promote the incorporation of Al in the C-(A)-S-H structure as they can charge-balance Al replacing Si in the bridging sites of the silicate chains, as observed for Portland cements with different alkali contents.[32] This is supported by atomistic simulations of alkali ions in C-(A)-S-H phases with a tobermorite-based structure, which indicate that highly stable phases can be achieved if the alkali ions are associated with a bridging Al(IV) site and a proper amount of H atoms for charge-balancing.[33] In contrast, for highly diluted solutions, as often used in syntheses of C-(A)-S-H phases, high pH values obtained in the presence of NaOH or KOH will stabilize $Al(OH)_4^-$ ions in solution, which lowers the Al uptake in C-(A)-S-H.[34] Cement hydration in alkaline solution results in a C-(A)-S-H phase with a higher degree of structural order, as seen by better resolved peaks in the

^{29}Si NMR spectra.[35] For C-(A)-S-H phases exposed to alkaline solutions, the alkali ions may absorb to the surface of the C-(A)-S-H particles[36] or interact directly with the Si–O sites in the interlayer, depending on their hydration energy.[37] It has been proposed that Na^+ and K^+ ions can partly replace interlayer Ca^{2+} ions, resulting in a more negative surface charge, shorter silicate chains and a reduction of the basal spacing of the interlayer.[31,38] Moreover, the replacement of Ca^{2+} by Na^+ or K^+ may result in an increased ^{29}Si NMR shielding of the SiO_4 units of the silicate chains, indicating that the alkali ions are in the near vicinity of the SiO_4 units. Experiments with variable Ca/Si ratios of the C-(A)-S-H phases, equilibrated with sodium or potassium hydroxide, indicate a reduction in the alkali uptake by C-(A)-S-H with increasing dissolved calcium concentrations.[31] Cation exchange measurements have shown that at low Ca/Si ratios, alkalis as well as some of the Ca^{2+} ions are readily exchangeable suggesting their presence in the diffuse layer, whereas at higher Ca/Si ratios only the alkali ions can be replaced.[39] These findings suggest a competitive relation between calcium and alkali ions in the interlayer of the C-(A)-S-H phases.

^{23}Na NMR has only been utilized in very few studies of C-S-H phases, which may reflect that the ^{23}Na chemical shift is less sensitive to structural changes beyond its hydration sphere. For C-S-H samples exposed to NaCl solutions, the broad resonance at approx. -10 ppm has been assigned to outer-sphere hydrated Na^+ ions, $Na(H_2O)_6^+$, on the C-S-H surface.[37] For C-(A)-S-H samples synthesized with $NaAlO_2$ as sodium and aluminium source, two distinct ^{23}Na sites have been observed at -7.6 ppm and -10 ppm and assigned to interlayer sodium sites interacting with octahedral and tetrahedral Al, respectively.[23] Moreover, two different ^{23}Na resonances have also been reported for sodium alumino-silicate hydrate (N-A-S-H) and sodium-modified calcium alumino-silicate hydrate (C-(N)-A-S-H) phases, synthesized under highly alkaline conditions, and ascribed to two different Na^+ environments associated with tetrahedral Al of Si-O-Al acid sites.[40,41] Thus, some ambiguities exist in the assignments of ^{23}Na resonances and the results indicate that the role of alkalis in C-S-H and C-(A)-S-H phases remains still not clear.

The aim of the present study is to probe the location and quantity of Al in the different environments of the C-(A)-S-H phase as a function of composition and alkali content, since this information will contribute to a better understanding of the structure and composition of C-(A)-S-H phases formed in Portland cement – SCM blends. C-(A)-S-H samples with Al/Si ratios of 0.05 – 0.20 and Ca/Si ratios in the range 0.6 – 1.6 have been prepared in 1.0 M NaOH solutions at ambient conditions by curing for time intervals of 3 and 15 months. In addition, C-(A)-S-H samples have been synthesized in 0.1 M and 0.5 M NaOH solutions to study the effect of alkali concentration on the

incorporation aluminium and sodium in the C-(A)-S-H phase. Multinuclear solid-state NMR (^{23}Na, ^{29}Si and ^{27}Al) is employed as the principal tool to characterize the nano-scale structure of the C-(A)-S-H phases and semi-quantitatively investigate the incorporation of aluminium and sodium in the structure. This includes ^{27}Al MAS NMR experiments performed at an intermediate (14.1 T) and very high magnetic field (22.3T) to unravel resonances from structurally distinct sites, utilizing the increase in chemical shift dispersion and the reduced second-order quadrupolar broadening on going to higher magnetic field. A convincing approach to quantify Al(IV) in the C-(A)-S-H structure is presented, which utilize information from both ^{27}Al and ^{29}Si NMR and employs a simulation approach that follows the basic alumino-silicate chain structure of the defect tobermorite model for C-(A)-S-H phases. Moreover, the role of alkalis on the incorporation of Al is different for low and high Ca/Si ratios, as a clear correlation between the sodium and aluminium uptake is only observed for C-(A)-S-H phases with short silicate chain lengths (*i.e.*, high Ca/Si ratios).

EXPERIMENTAL SECTION

Sample preparation. The C-(A)-S-H samples were prepared by mixing SiO_2, CaO and $CaAl_2O_4$, targeting the molar ratios of Ca/Si_{init} = 0.6, 0.8, 1.0, 1.2, 1.4, 1.6 and Al/Si_{init} = 0.05, 0.10, 0.15 and 0.20, in equilibrium with 1.0 M NaOH solutions for curing times of 3 and 15 months. In addition, samples with 0.1 M and 0.5 M NaOH solutions have been prepared for the Ca/Si ratios of 0.8 and 1.0. All syntheses used a solution/solid ratio of 45 and all preparations were conducted in a N_2-filled glove box at ambient temperature (~20°C). SiO_2 (Aerosil 200) was provided by Evonik and used as received. CaO was obtained by burning $CaCO_3$ (Merck, pro analysis) at 1000 °C for 12 hours. $CaAl_2O_4$ was obtained by the sintering reaction of $CaCO_3$ and Al_2O_3 in a furnace at increasing temperatures of 800 ºC (1 h), 1000 ºC (4 h) and 1400 ºC (8 h), followed by cooling with a rate of 600 ºC/h. The reaction mixtures were stored in 100 mL PE-HD containers which were placed on a horizontal shaker (rate of 100 rpm) at ambient temperature (~20°C). After curing times of 3 and 15 month, the solid and liquid phases were separated by filtration through a 0.45 µm nylon filter and the solid phase was washed with a 50% v/v water - ethanol solution and secondly with a 94 vol.% ethanol solution. The samples were lyophilized for 7 days and stored in N_2 filled desiccators with saturated $CaCl_2$ solutions (RH ≈ 30%) and NaOH as a CO_2 trap.[31]

The elemental concentrations of calcium, silicon, sodium, and aluminum in the filtrates were determined with a Dionex DP ICS-3000 ion chromatograph. The liquid samples were diluted by factors of 1 – 1000 to reach concentrations in the range of 0.1 – 50 mg/L, thereby allowing detection

of concentrations up to 50,000 mg/L. The estimated error from sample preparation, dilution and measurement was ≤ 10%. The real, bulk Al/Si ratios of the C-(A)-S-H samples were obtained by mass balance calculations using these data for the solution and the Al and Si contents of the starting materials. The Na contents bound in the C-(A)-S-H were determined by a direct method[31] where 20 mg of the solid sample was dissolved in 10 mL of a 0.1 M HCl solution, which was analyzed by ion chromatography.

Solid-state NMR. The single-pulse ^{29}Si MAS NMR experiments were carried out on a Bruker-400 (9.39 T) spectrometer using a Bruker ^{1}H-X 4 mm MAS probe for a spinning speed of ν_R = 10.0 kHz The spectra used a pulse length of 1.75 μs for an rf field strength of $\gamma B_1/2\pi$ = 71 kHz, a recycle delay of 30 s, and 2048 scans. The cross-polarization ^{29}Si{^{1}H} CP/MAS NMR spectra were obtained with the same probe, employing a spinning speed of ν_R = 4.0 kHz. The spectra used a ^{29}Si rf field strength of $\gamma B_1/2\pi$ = 46 kHz for CP contact times in the range 0.05 – 8.0 ms and a ^{1}H rf field strength of $\gamma B_2/2\pi$ = 50 kHz for the initial excitation (90^{o} pulse, 5.0 μs), the CP contact time, and the high-power ^{1}H decoupling during acquisition. ^{29}Si chemical shifts are referenced to tetramethylsilane (TMS), using an external sample of β-Ca_2SiO_3 (δ_{iso} = -71.33 ppm)[42] as a secondary reference. The simulations of the ^{29}Si MAS and ^{29}Si{^{1}H} CP/MAS NMR spectra were performed by the DMFit software.[43]

The ^{27}Al MAS NMR spectra were recorded on a Varian Direct-Drive VNMR-600 spectrometer (14.09 T) using a home-built CP/MAS probe for 4 mm o.d. zirconia rotors and ν_R = 13.0 kHz, a recycle delay of 2 s, and 4096 scans. A short excitation pulse of τ_p = 0.5 μs for an rf field strength of $\gamma B_1/2\pi$ = 60 kHz was employed in order to be in the linear regime where the central transition intensities are quantitatively reliable for sites experiencing different quadrupolar couplings, *i.e.*, $\tau_p \leq \pi/[2(I + 1/2)]$.[44] In addition, a series of ^{27}Al NMR experiments have been conducted on a narrow-bore Bruker 950/54 us^2 magnet (22.3 T) with a Bruker AVANCE III HD console, using a triple-resonance ^{1}H-X-Y 2.5 mm MAS probe. The single-pulse experiments employed ν_R = 20.0 kHz, a pulse width of 0.5 μs for an ^{27}Al rf field of $\gamma B_1/2\pi$ = 89 kHz, a recycle delay of 2 s, and 8192 scans. The ^{27}Al{^{1}H} CP/MAS NMR spectra employed a CP contact time of 50 μs, an ^{27}Al rf field strength of $\gamma B_1/2\pi$ = 60 kHz for the CP contact and ^{1}H rf field strengths of $\gamma B_2/2\pi$ = 90 kHz for the initial ^{1}H excitation pulse and CP contact time and $\gamma B_2/2\pi$ = 72 kHz for the decoupling during acquisition. The CP contact time was optimized for one of the samples and the rather short value agrees well with the contact time of maximum intensity observed in ^{27}Al{^{1}H} CP/MAS NMR experiments on other cementitious materials.[21] For all single-pulse ^{27}Al NMR experiments, low-intensity signals observed

in spectra of the empty rotors and probe background have been subtracted prior to the quantitative analysis.

^{27}Al MQMAS NMR spectra have been recorded at 14.09 T and 22.3T, using the same probes as described above and the three-pulse *z*-filter pulse sequence.[45] The excitation and conversion pulses correspond to 180° and 60° liquid pulses, respectively, for ^{27}Al (I = 5/2)[46] ($\gamma B_1/2\pi$ = 60 kHz at 14.09 T and $\gamma B_1/2\pi$ = 89 kHz at 22.3 T), whereas the central-transition selective *z*-pulse had a length of 2.5 μs ($\gamma B_1/2\pi$ = 33 kHz) at 14.09 T and of 7 μs ($\gamma B_1/2\pi$ = 13.5 kHz) at 22.3 T. Spectral widths of 39 kHz (14.09 T) and 50 kHz (22.3 T) were used in both dimensions, corresponding to $3\nu_R$ and $2\nu_R$, together with 64 t_1 (14.09 T) and 96 t_1 (22.3 T) increments and a 1-s relaxation time. The frequencies in the isotropic (F_1) dimension are scaled and referenced as triple-quantum shifts, $\delta_{3Q} = (\nu_i + (3 - k)\Delta)/((1 + k)\nu_L)$, where ν_i is the observed F_1 resonance frequency, Δ is the transmitter offset relative to the spectral reference and k = 19/12 for I = 5/2 in the triple-quantum MAS experiment.[47] The ^{27}Al chemical shifts are referenced to a 1.0 M aqueous solution of $AlCl_3 \cdot 6H_2O$.

The ^{23}Na MAS NMR spectra were acquired at 14.09 T, using similar conditions as described above for the ^{27}Al NMR experiments; ν_R = 12.0 kHz, 0.5 μs excitation pulse ($\gamma B_1/2\pi$ = 60 kHz), 4-s relaxation time and 1024 scans. The ^{23}Na chemical shifts are relative to a 1.0 M aqueous solution of NaCl.

RESULTS AND DISCUSSION

Characterization of C-(A)-S-H samples by ^{29}Si and ^{27}Al MAS NMR. The lack of long-range order in the C-(A)-S-H structure impedes detailed structural studies of these phases by conventional powder X-ray diffraction techniques. However, for these systems high-resolution solid-state NMR can provide valuable structural information as the ^{27}Al and ^{29}Si chemical shifts depend primarily on the coordination state and bonding network within the nearest coordination spheres. This has been utilized in a wide range of solid-state NMR studies of C-(A)-S-H phases, where some of the main features are illustrated in Figure 1 by ^{29}Si and ^{27}Al NMR spectra of the C-(A)-S-H samples synthesized with the initial ratio Ca/Si = 0.8, initial Al/Si ratios ranging from 0.05 to 0.20 and cured in 0.1, 0.5, and 1.0 M NaOH solutions for three months. The ^{29}Si NMR spectra generally resolve three main peaks at roughly -79, -81 and -85 ppm, corresponding to the Q^1, $\mathbf{Q_p^2(1Al_{IV})}$ and Q^2 sites of the dreierketten silicate chains, which are connected to the main CaO_2 layer on both sides. These frequencies may shift slightly depending on the Ca/Si ratio[48,49] and the alkali concentration.[27,37] Moreover, the Q^2 resonance contain contributions from the pairing and bridging sites, $\mathbf{Q_p^2}$ and $\mathbf{Q_b^2}$,

which resonate at approx. -85 ppm and -83 ppm for Al-free C-S-H samples[49] but are generally not resolved for C-(A)-S-H samples due to the partial overlap with the $\mathbf{Q_p^2(1Al_{IV})}$ peak. A schematic representation of the C-(A)-S-H structure at low Ca/Si ratio (*e.g.*, Ca/Si = 0.8) is shown in Figure 2, which includes the fundamental silicate units and tetrahedral Al sites that form the starting point for the present study.

The ^{27}Al NMR spectra clearly resolve resonances from Al in tetrahedral (50 – 80 ppm) and octahedral (0 – 20 ppm) coordination, where experiments at high magnetic field allow distinction of different Al(IV) and Al(VI) species as a result of the increased chemical shift dispersion and reduction in second-order quadrupolar broadening. For the ^{27}Al NMR spectra in Figure 1, the tetrahedral resonances at 74 and 68 ppm are ascribed to Al(IV) in the bridging sites of the silicate chains whereas the minor resonance at 61 ppm is ascribed to a small amount of strätlingite,[50,51] formed as a minor secondary product under the actual synthesis and curing conditions. Narrow resonances are also observed in the octahedral region at 12.3 ppm, 10.5 – 10.8 ppm, and 5 ppm which correspond to minor amounts of secondary phases such as katoite/silicious hydrogarnet (δ_{iso}(Al) = 12.2 – 12.4 ppm),[52,53] hydroxy-AFm ($Ca_4Al_2(OH)_{14}\cdot 6H_2O$, 10.2 ppm),[52] $CaAl_2(OH)_8\cdot 6H_2O$ (10.2 ppm),[54] $Ca_2Al_2(OH)_{10}\cdot 3H_2O$ (10.3 ppm),[52] the Al(VI) site of strätlingite (11.3 ppm)[50,51] and the Al(VI) site associated with the C-(A)-S-H phase (5.0 ppm).[21,25] Generally, the fraction of the secondary aluminate phases are highest at high Al/Si ratio or low pH (*i.e.*, 0.1 M NaOH).

The aluminium incorporated in the bridging sites of the silicate structure is observed by both the Al(IV) resonances in the ^{27}Al NMR spectra and by the $\mathbf{Q_p^2(1Al_{IV})}$ peak in the ^{29}Si NMR spectra. A linear correlation between the intensities of these resonances has earlier been reported for C-(A)-S-H phases formed in white Portland cements hydrated for different times and in $NaAlO_2$ solutions of different concentration.[18] However, this correlation considered only relative amounts of Al(IV) in the C-(A)-S-H phase and to further investigate the origin of the $\mathbf{Q_p^2(1Al_{IV})}$ resonance in the ^{29}Si NMR spectra, which may potentially also reflect coordination to Al in different coordination states, the first goal of the present study is to establish a quantitative correlation between the intensities of the ^{27}Al and ^{29}Si NMR resonances associated with Al incorporated in the C-S-H structure.

Simulations of the ^{29}Si NMR spectra. In the subsequent analysis, we initially focus on the C-(A)-S-H samples synthesized with an initial Al/Si = 0.10 in 1.0 NaOH solutions and with different Ca/Si ratios (0.6 – 1.6), as these samples contain the lowest amounts of secondary phases. Following the defect tobermorite model for the C-(A)-S-H structure,[9-12] a minimum of four resonances are required

to simulate the ^{29}Si NMR spectra corresponding to the Q^1, $Q_p^2(1Al_{IV})$, Q_b^2, and Q_p^2 sites. However, an additional resonance at lower frequency needs also consideration to account for the intensity in the -85 to -88 ppm region. Based on the $^{29}Si\{^1H\}$ CP/MAS NMR experiments presented below, we assign this resonance to a second type of paired Q^2 sites in the structure. Thus, the simulations include peaks from a dominating Q^2 site at -84.3 ppm, denoted Q_{pa}^2, and for a less intense site at -86.7 ppm, Q_{pb}^2. Moreover, as the $Q_p^2(1Al_{IV})$ resonance overlaps significantly with the Q^1 and Q_b^2 peaks, the frequency and linewidth of the $Q_p^2(1Al_{IV})$ resonance is restricted to $\delta(^{29}Si)$ = -80.8 ± 0.1 ppm and *FWHM* = 2.1 ppm, following similar analyses of the C-(A)-S-H phase formed in hydrated Portland cements,[32,51] where this restriction has resulted in sound measures of the relative peak intensities. Furthermore, the defect-tobermorite model implies that the bridging and paired SiO_4 tetrahedra must be present in an intensity ratio of $I(Q_p^2)/I(Q_b^2)$ = 2, which is implemented as a restriction in the simulations (with $I(Q_p^2)$ = $I(Q_{pa}^2)$ + $I(Q_{pb}^2)$), as also used in recent studies of C-(A)-S-H phases equilibrated at 20 °C[31] or at different temperatures.[55] The peak shapes are fixed to 0.5/0.5 fractions of Gaussian/Lorentzian line shapes, following our experience from previous simulations of C-(A)-S-H phases[32,49,51] and providing a uniform profile for the individual peaks. Moreover, the linewidths are only allowed to vary over a relative narrow range, corresponding to *FWHM* = 1.9 to 3.0 ppm. In the recent atomistic modelling and DNP-enhanced NMR study of synthesized C-(A)-S-H samples by Kunhi Mohamed *et al.*,[25] a two-dimensional $\{^{29}Si\}^{27}Al$ refocused dipolar INEPT MAS spectrum of a C-(A)-S-H phase (Ca/Si = 2.0 and Al/Si = 0.07) showed that the Al(VI) resonance at 5.0 ppm is associated with ^{29}Si sites with a chemical shift of -77 ppm. A resonance at -77 ppm is not apparent in the present ^{29}Si NMR spectra and it is not considered at this stage in the simulations, as it will not overlap with the $Q_p^2(1Al_{IV})$ resonance at -80.8 ppm and thereby influence the intensity for this peak derived from the simulations (the -77 ppm resonance is considered in more detail in a following section).

The optimized simulations by least-squares fitting to the experimental spectra are illustrated for the Ca/Si = 0.6 and Ca/Si = 0.8 samples in Figure 3, whereas the corresponding deconvolutions for Ca/Si = 1.0 – 1.6 are given in Figure S1. Convincing simulations are generally achieved by this approach (Figures 3 and S1), resulting in rather small variations in peak positions and linewidths, as shown by their ranges for the individual peaks in Table 1. The simulations provide the relative intensities of the Q^1, $Q_p^2(1Al_{IV})$, Q_b^2, Q_{pa}^2 and Q_{pb}^2 peaks listed in Table 2 for the C-(A)-S-H samples synthesized with Al/Si = 0.10 and cured in 1.0 M NaOH solutions. These intensities allow calculation of the mean chain length of alumino-silicate tetrahedra ($\overline{CL}_{IV}$) and pure silicate tetrahedra ($\overline{CL}_{Si}$) as well as the Al/Si ratio of the alumino-silicate chains (Al_{IV}/Si), using the expressions[56-58]

$$\overline{CL}_{IV} = \frac{2[Q^1 + Q^2_{pa} + Q^2_{pb} + Q^2_b + \frac{3}{2}Q^2_p(1Al_{IV})]}{Q^1} \quad (1)$$

$$\overline{CL}_{Si} = \frac{2[Q^1 + Q^2_{pa} + Q^2_{pb} + Q^2_b + Q^2_p(1Al_{IV})]}{[Q^1 + Q^2_p(1Al_{IV})]} \quad (2)$$

$$Al_{IV}/Si = \frac{Q^2_p(1Al)}{2[Q^1 + Q^2_{pa} + Q^2_{pb} + Q^2_b + Q^2_p(1Al_{IV})]} \quad (3)$$

The calculated Al/Si ratios of the C-(A)-S-H samples (Table 2) are all below the ratio (0.10) used in the syntheses, which reflect the presence of secondary phases and/or that the $Q^2_p(1Al)$ peak in the ^{29}Si NMR spectra does not account for all aluminium in the C-(A)-S-H phase. Moreover, the mean chain lengths show the expected decrease with increasing Ca/Si ratio, following earlier studies of similar phases and reflecting the sequential removal of Si from the bridging sites.[12,29,49]

Assignment of the ^{29}Si NMR resonance at -87 ppm. Satisfactory simulations of the ^{29}Si NMR spectra for the C-(A)-S-H phases (Figures 3 and S1) require inclusion of a resonance at approx. -87 ppm (denoted in this work as Q^2_{pb}), in agreement with earlier ^{29}Si NMR studies of synthesized C-S-H[59,60] and C-(A)-S-H phases[27,28,31] as well as hydrated Portland cements.[60,61] Le Saoût *et al.*[61,62] and L'Hôpital *et al*.[27,28,31] denoted this resonance as the 'Q^2_u peak', which is ascribed to a bridging tetrahedron connected to another bridging tetrahedron in a neighboring silicate chain via H – H bonding, following the assignment in an early ^{29}Si NMR study of synthesized tobermorites by Sato and Grutzek.[59] Thus, interlayer H – H bonding should result in a shift of the Q^2_b resonance by approx. 4 ppm to lower frequency. Moreover, Klur *et al*. have studied a ^{29}Si enriched C-S-H synthesized with Ca/Si = 0.8 by single-pulse ^{29}Si NMR as well as a two-dimensional broadband dipolar recoupling (BDR) sequence.[60] They observed a minor resonance at -87.3 ppm, which according to the BDR experiment was coupled to a site with chemical shift at -91.5 ppm, corresponding to a Q^3 site. Thus, the -87.3 ppm resonance, which they denoted Q^2_v, was assigned to a pairing SiO_4 tetrahedron bonded to a Q^3 site that connects bridging sites between two different silicate chains. However, the relative intensities of both peaks were rather low (3.5% and 1.5% for the Q^2_v and Q^3 peaks, respectively),[60] and any indications of Q^3 sites in the present C-(A)-S-H samples have not been observed (*c.f.* Figures 1 and 3). Moreover, Klur *et al*. observed indications of two different Q^2 bridging sites at -82.1 ppm and -83.9 ppm, which they denoted Q^2_p and Q^2_i and proposed to originate from sites where the two non-bonding oxygens are associated with two H atoms and a H and a Ca atom, respectively. The

frequency of -82.1 ppm is in good agreement with the chemical shift range observed for the Q_b^2 sites in the present analysis (*c.f.*, Table 1), however, the resolution in the present spectra does not allow any distinction of different types of Q_b^2 sites.

To investigate the assignment of the -87 ppm resonance in more detail, we have studied the C-(A)-S-H sample prepared with Ca/Si = 0.8 and Al/Si = 0.10 in a 1.0 M NaOH solution by $^{29}Si\{^1H\}$ cross-polarization (CP)[63] NMR, which selectively detects Si sites with H atoms in their near environment and gives a signal enhancement that strongly depends on the ^{29}Si–^1H dipolar interaction and thereby the hydrogen network around the Si nuclei. $^{29}Si\{^1H\}$ CP/MAS NMR spectra with 14 different CP contact times in the range 0.05 – 8.0 ms have been acquired (Figure 4) and simulated using the approach described in the previous section, however, without the requirement of $I(Q_p^2)/I(Q_b^2)$ = 2. An additional resonance at -76.0 ppm (*FWHM* = 3.0 ppm) was included in the simulations, corresponding to hydroxylated monomeric silicate units (Q_H^0; *e.g.*, $(HO)_xSiO_{4-x}$ sites), which are strongly enhanced in the $^{29}Si\{^1H\}$ CP/MAS NMR experiments, despite not clearly resolved in the direct-polarization, single-pulse ^{29}Si NMR spectra. This agrees well with earlier $^{29}Si\{^1H\}$ CP/MAS NMR studies of hydrated Ca_3SiO_5 samples[64-66] where the Q_H^0 species were found to constitute 2 - 5 % of the overall ^{29}Si NMR intensity. An example of a simulated $^{29}Si\{^1H\}$ CP/MAS NMR spectrum is illustrated in Figure S2, whereas the resulting ^{29}Si intensities for the different sites are shown in Figures 5 and S3 as function of the CP contact time. These CP curves are analyzed using a classical inverse spin-temperature approach[63,67] for the build-up and decay of Si magnetization ($M_x(\tau_{cp})$) as a function of the contact time (τ_{cp}), assuming the ^{29}Si spins being diluted relative to the ^1H spins, a condition fulfilled for samples with ^{29}Si in natural abundance. Moreover, the rotating-frame relaxation of the ^{29}Si spins is assumed to be much longer than the corresponding ^1H rotating-frame relaxation ($T_{1\rho}^{Si} >> T_{1\rho}^{H}$), resulting in the following expression for $M_x(t = \tau_{cp})$:

$$M_x(t) = \frac{M^H(0)}{1-T_{SiH}/T_{1\rho}^H} \exp(-\frac{t}{T_{1\rho}^H})[1 - \exp\left(\left(\frac{1}{T_{1\rho}^H} - \frac{1}{T_{SiH}}\right)t\right)] \quad (4)$$

Here, $M^H(0)$ is the ^1H magnetization after the 90° ^1H pulse and T_{SiH} is the time constant describing the build-up of $^1H \rightarrow {}^{29}Si$ magnetization, which depends on the ^1H – ^{29}Si dipolar interaction, with T_{SiH} being proportional to $1/(r_{Si\text{-}H})^6$ of the internuclear distance ($r_{Si\text{-}H}$).[63,68] This approach has been successfully employed in $^{29}Si\{^1H\}$ CP/MAS NMR studies of hydrated Ca_3SiO_5,[65,66] C-S-H phases[69,70] and other cementitious systems.[71] Eq. (4) allows determination of $M^H(0)$, T_{SiH} and $T_{1\rho}^H$ by least-

squares fitting to the experimental intensities as function of τ_{cp}, providing the T_{SiH} and $T_{1\rho}^{H}$ time constants listed in Table 3 for the different sites of the C-(A)-S-H phase.

The resonance at -87 ppm (denoted Q_{pb}^2 in Table 3) exhibits T_{SiH} and $T_{1\rho}^{H}$ time constants that are very similar to those for the pairing site, Q_{pa}^2, as well as the pairing site bonded to Al in the bridging site ($Q_p^2(1Al_{IV})$), whereas both parameters are much smaller than those observed for the bridging site, Q_b^2. The shorter T_{SiH} values indicate that the site of the -87 ppm peak has ^{1}H atoms in closer distance than the Q_b^2 site, whereas the longer $T_{1\rho}^{H}$ value for Q_b^2 indicates a more rigid ^{1}H network for this silicate site as compared to the -87 ppm peak and the two pairing sites, Q_{pa}^2 and $Q_p^2(1Al_{IV})$. Thus, the close similarity in these parameters for the site of the -87 ppm resonance with those of the Q_{pa}^2 and $Q_p^2(1Al_{IV})$ sites strongly suggests that the -87 ppm resonance originates from a Q^2 pairing site of the same type as seen by the intense resonance at approx. -84 ppm (*i.e.*, Q_{pa}^2). Thus, we assign the -87 ppm resonance to a second type of Q^2 pairing site, denoted Q_{pb}^2, which may exhibit a slightly different local geometry compared to the Q_{pa}^2 site that can account for the shift of approx. 2 ppm to lower frequency. The Q_{pb}^2 site is only observed for C-(A)-S-H phases with low Ca/Si ratio, which are characterized by relatively long average alumino-silicate chains and pure silicate chains (Table 2) and thereby not only composed of silicate dimers and pentamers. Thus, the Q_{pb}^2 site may potentially be assigned to pairing Q_p^2 sites in the middle of octameric or longer silicate chains and thereby the Q_p^2 sites in between two bridging (Q_b^2) sites. The assignment of the -87 ppm peak to a Q^2 pairing site is used in the previous and subsequent sections and impacts the quantitative evaluation of the single-pulse ^{29}Si NMR spectra as $[I(Q_{pa}^2) + I(Q_{pb}^2)]/I(Q_b^2) = 2$ is assumed. Finally, it is noted that a resonance at -88 ppm has been observed for alkali-activates pastes containing calcium-(sodium) aluminosilicate hydrate (C-(N)-A-S-H) and sodium aluminosilicate hydrate (N-A-S-H) gels which was assigned to Q^3(1Al) and Q^4(4Al) sites in these hydrates.[41,72] In this study the -87 ppm resonance has been identified in C-(A)-S-H samples with different Al/Si ratios (0.05, 0.10, 0.15 and 0.20) and synthesized with different NaOH concentrations (0.5 and 1.0 M) but only for Ca/Si ratios of 0.6 and 0.8. This shows that the environment for the Q_{pb}^2 site is independent of the Al concentration and thereby does not originate from minor amounts of C-(N)-A-S-H and N-A-S-H phases in our samples.

Al/Si ratios from ^{27}Al NMR. ^{27}Al MAS NMR spectra of the C-(A)-S-H samples synthesized with Al/Si = 0.10 in 1.0 NaOH solutions and with different Ca/Si ratios (0.6 – 1.6), are shown in Figure 6 and illustrate the observation of well-separated resonances from Al(IV), Al(V), and Al(VI). The line shapes for the Al(IV) peaks indicate at least three different types of Al(IV) sites, depending on the

Ca/Si ratio, which will be analyzed in more detail below. Five-fold coordinated Al is observed by the peak at 35 ppm for the samples with Ca/Si = 1.0 and above, which also contain the resonance at 5.0 ppm from Al(VI) associated with the C-(A)-S-H phase. In addition, small Al(VI) resonances from minor secondary phases such as katoite/siliceous hydrogarnet (12.3 – 12.4 ppm)[52,53] and calcium aluminate hydrates ($CaAl_2(OH)_8 \cdot 6H_2O$, $Ca_2Al_2(OH)_{10} \cdot 3H_2O$ and $Ca_4Al_2(OH)_{14} \cdot 6H_2O$; 10.2 – 10.6 ppm)[52,54] are also observed. The fraction of Al(IV), Al(V) and Al(VI) are determined by spectral integration (Table 4) where the relative intensities for Al(VI) has been further divided into contributions from the secondary phases and the 5.0 ppm resonance by spectral simulations of the octahedral region. These simulations used a combination of Gaussian and Lorentzian line shapes for the individual peaks, which is an acceptable approach considering the high magnetic field and the presence of small ^{27}Al quadrupolar interactions ($C_Q < 1.5$ MHz) for the contributing phases.[18,52] Direct measures for the bulk Al/Si ratios of the C-(A)-S-H phases (Table 4) are obtained from mass-balance calculations using the Al/Si ratio of the starting materials and the Al and Si concentrations in the solutions (after three month curing) determined by ion chromatography. This approach reveals that the bulk Al/Si values of the solids are all close to the initial Al/Si = 0.10 ratio used in the syntheses. Combining the bulk Al/Si ratios with the intensity fractions from ^{27}Al NMR allows calculation of the Al(IV)/Si, [Al(IV) + Al(V)]/Si, [Al(IV) + Al(VI)]/Si, and [Al(IV) + Al(V) + Al(VI)]/Si ratios for aluminum associated with the C-(A)-S-H phases (*i.e.*, Al(VI) corresponds to the relative intensity of the 5.0 ppm resonance). These ratios are used in the graphs of Figure 7a – d, which illustrate the corresponding Al_{IV}/Si ratios from ^{29}Si NMR, determined from Eq. (3), as a function of these ratios. The graphs reveal 1:1 correlations between the ^{27}Al and ^{29}Si NMR data for the Al(IV)/Si and [Al(IV) + Al(V)]/Si ratios from ^{27}Al NMR, with the most convincing correlation being observed for the Al(IV)/Si data (Figure 7a). The two correlations are further examined in Figure 8 by including data for 26 additional C-(A)-S-H samples, synthesized at the same conditions but at different initial Ca/Si (0.6 – 1.6) and Al/Si (0.05 – 0.20) ratios with 0.5 or 1.0 M NaOH concentrations for three or 15 months (see Figure S4 for further details on the specific C-(A)-S-H compositions). The graphs show convincing 1:1 correlations between both the Al(IV)/Si and [Al(IV) + Al(V)]/Si ratios from ^{27}Al NMR and the Al_{IV}/Si ratios from ^{29}Si NMR, as supported by the following results from linear regression analysis.

$$(Al_{IV}/Si)_{Si} = (0.952 \pm 0.019)\ (Al(IV)/Si)_{Al} + (0.005 \pm 0.002) \qquad R^2 = 0.989 \qquad (5)$$

$$(Al_{IV}/Si)_{Si} = (0.951 \pm 0.020)\ ([Al(IV) + Al(V)]/Si)_{Al} + (0.002 \pm 0.002) \qquad R^2 = 0.987 \qquad (6)$$

Moreover, inclusion of the ^{27}Al NMR intensities for Al(VI) in the correlation using all data (Figure S4) clearly supports the results in Figure 7c, showing no correlation between $(Al_{IV}/Si)_{Si}$ and the [Al(IV) + Al(VI)]/Si ratio from ^{27}Al NMR. No preference between the two correlations based on the data in Figure 8 can be made, which is ascribed to the precision of the measured Al/Si ratios, *e.g.* ±0.01 for $(Al_{IV}/Si)_{Si}$. In addition, the fraction of Al(V) is generally low in the present C-(A)-S-H samples, *i.e.*, Al(V)/Al(IV) ≤ 0.16 for all samples, implying that it only makes small changes to Al(IV)/Si. Thereby, the 1:1 correlations in Figures 7 and 8 reveal that the $Q_p^2(1Al_{IV})$ ^{29}Si NMR resonance at approx. -81 ppm is associated with four-fold coordinated Al and potentially also five-fold coordinated Al in the bridging site of the silicate chain structure. Earlier studies have proposed that the Al(V) species are present in the interlayer of the C-S-H structure,[17,21,22,23] whereas its specific presence in the bridging site of the silicate chains has recently been predicted by atomistic simulations (DFT calculations), supported by the observation of the Al(V) resonance (35 ppm) in a ^{29}Si filtered DNP-enhanced ^{27}Al CP/MAS NMR spectrum of a synthesized C-(A)-S-H sample with Ca/Si = 2.0 and Al/Si = 0.04.[25] According to the latter study, the Al(V) site should include two Al-O-Si bonds,[25] as present for the bridging Al(IV) sites, and such a $[(SiO)_2Al(OH)_{3-x}(H_2O)_x]$ environment is compatible with the findings in Figure 8b, which indicates that Al(V) in the bridging site can also lead to a 3.5 ppm shift to higher frequency for the neighboring Q^2 pairing site (*i.e.*, the shift difference between $Q_p^2(1Al_{IV})$ and Q_{pa}^2, Table 1). In contrast to the qualitative correlation between the Al(IV) intensity observed by ^{27}Al NMR and the intensity of the $Q_p^2(1Al_{IV})$ resonance from the simulations of the ^{29}Si NMR spectra reported earlier,[18] the 1:1 correlation in Figure 8a is quantitative, implying that reliable Al(IV)/Si ratios can be derived both from the ^{27}Al and ^{29}Si NMR spectra.

The Al(VI) resonance at 5.0 ppm associated with C-(A)-S-H. From the plots of $(Al_{IV}/Si)_{Si}$ as a function of $([Al(IV) + Al(VI)]/Si)_{Al}$ in Figure 7c, and in Figure S4 for the 32 C-(A)-S-H samples, it is apparent that the $Q_p^2(1Al_{IV})$ resonance in the ^{29}Si NMR spectra cannot account for octahedrally coordinated Al (5.0 ppm resonance) associated with the C-(A)-S-H phase. This is in full agreement with the recent atomistic modelling and DNP-enhanced NMR study by Kunhi Mohamed *et al.*,[25] where a two-dimensional $\{^{29}Si\}^{27}Al$ refocused dipolar INEPT MAS spectrum of a C-(A)-S-H phase (Ca/Si = 2.0 and Al/Si = 0.07) showed that the Al(VI) resonance at 5.0 ppm is associated with a ^{29}Si site with a chemical shift of -77 ppm, in addition to the expected strong correlation peak between Al(IV) and the ^{29}Si $Q_p^2(1Al_{IV})$ resonance at -81 ppm. The atomistic modelling predicted that Al(VI) should be present in the bridging site of the silicate chains, forming a site of the type $[(SiO)_2Al(OH)_4]$,

corresponding to a $Q_p^2(1Al_{VI})$ site in the ^{29}Si NMR spectra. Clear indications of a resonance at -77 ppm are not observed in the ^{29}Si NMR spectra of the synthesized C-(A)-S-H samples in the present work as this resonance will significantly overlap with the Q^1 resonance at -78.4 ppm, which dominates the spectra for samples with high Ca/Si ratio. However, a high-frequency shoulder to this resonance may be identified in the ^{29}Si NMR spectrum of a C-(A)-S-H sample, synthesized with Ca/Si = 1.6, Al/Si = 0.05 and equilibrated in water for one year by L'Hôpital *et al.*,[28] which also showed a high fraction of Al(VI) in the structure, as evidenced by ^{27}Al NMR.

The presence of a $Q_p^2(1Al_{VI})$ resonance will affect the simulation approach of the ^{29}Si NMR spectra and thereby the mean chain length of alumino-silicate tetrahedra ($\overline{CL}$) and pure silicate tetrahedra ($\overline{CL}_{Si}$) as well as the Al/Si ratio of the alumino-silicate chains (Al/Si) calculated from the relative intensities of the ^{29}Si resonances (Eqs. 1 – 3). However, although not resolved, the $Q_p^2(1Al_{VI})$ resonance can be considered in the simulations, since its expected intensity can be derived from the relative intensities of the Al(IV) and Al(VI) resonances observed in the corresponding ^{27}Al NMR spectra. This approach has been implemented in the simulations and are illustrated in Figure 9 for the ^{29}Si NMR spectra of the C-(A)-S-H samples with Ca/Si = 1.2 and 1.4 (Al/Si_{init} = 0.10), which exhibit the highest fraction of Al(VI) according to ^{27}Al NMR (Table 4). The simulations use the same restrictions for the -77 ppm peak, as employed for the $Q_p^2(1Al_{IV})$ resonance at -80.8 ppm, and employ a fixed intensity ratio for the $Q_p^2(1Al_{VI})$ and $Q_p^2(1Al_{IV})$ peaks, corresponding to the $Al(VI)_{5ppm}/Al(IV)$ ratio determined by ^{27}Al NMR (*i.e.*, a fixed ^{29}Si chemical shift at -77.0 ppm and a linewidth of *FWHM* = 2.1 ppm). With these restrictions and those implemented in the previous section (*e.g.*, $[I(Q_{pa}^2) + I(Q_{pb}^2)]/I(Q_b^2) = 2$), the intensities of the individual resonances were optimized to the experimental spectra, where the simulated spectra are shown in Figure 9 and the resulting intensities summarized in Table 5.

The intensity of the $Q_p^2(1Al_{VI})$ resonance needs consideration in the calculations of the average alumino-silicate chain lengths and the Al/Si ratios, and assuming Al(VI) being present in a bridging site results in the following modifications of the expressions in Eqs. 1 – 3:

$$\overline{CL}_{IV+VI} = \frac{2[Q^1 + Q_{pa}^2 + Q_{pb}^2 + Q_b^2 + \frac{3}{2}\{Q_p^2(1Al_{IV}) + Q_p^2(1Al_{VI})\}]}{Q^1} \quad (7)$$

$$\overline{CL}_{Si*} = \frac{2[Q^1 + Q_{pa}^2 + Q_{pb}^2 + Q_b^2 + Q_p^2(1Al_{IV}) + Q_p^2(1Al_{VI})]}{[Q^1 + Q_p^2(1Al_{IV}) + Q_p^2(1Al_{VI})]} \quad (8)$$

$$Al_{IV+VI}/Si = \frac{Q_p^2(1Al_{IV}) + Q_p^2(1Al_{VI})}{2[Q^1 + Q_{pa}^2 + Q_{pb}^2 + Q_b^2 + Q_p^2(1Al) + Q_p^2(1Al_{VI})]} \quad (9)$$

These measures are also summarized in Table 5, where the values for $\overline{CL}_{IV+VI}$ show a prolongation of the alumino-silicate chains, as expected, when comparing these values with $\overline{CL}_{IV}$ in Table 2. For the pure silicate chain lengths, the values for $\overline{CL}_{Si}$ (Table 2) and $\overline{CL}_{Si*}$ (Table 5) are almost identical, in accordance with Eq. (8), when it considered that the $Q_p^2(1Al_{VI})$ intensity reduce the intensity of the Q^1 peak. The Al_{IV+VI}/Si values (Table 5) are obviously larger than the Al_{IV}/Si values, and in particular at high Ca/Si ratios. Interestingly, the Al_{IV+VI}/Si ratios are very similar (0.76 – 0.87) for all samples and thereby independent of the Ca/Si ratio, at least for samples prepared in alkaline solutions. This may reflect that the uptake of Al in the C-(A)-S-H phase depends mainly on the Al solution concentration, as proposed in an earlier studies of equilibrated C-(A)-S-H samples.[26,27] The ^{29}Si NMR spectra of the 26 additional C-(A)-S-H samples that formed the basis for the correlations in Figure 8 have been re-examined considering the contribution from the $Q_p^2(1Al_{VI})$ resonance at -77 ppm. Comparison of the calculated Al_{IV+VI}/Si ratios from these simulations (Eq. (9)) with those derived from ^{27}Al NMR shows a convincing correlation (Figure S5), corresponding to the equation:

$$(Al_{IV+VI}/Si)_{Si} = (0.95\ 0\pm\ 0.023)\ (Al_{IV+VI}/Si)_{Al} + (0.006 \pm 0.002) \qquad R^2 = 0.982 \qquad (10)$$

In an attempt to observe a clear reflection of the ^{29}Si resonance at -77 ppm, assigned to $Q_p^2(1Al_{VI})$ sites, we have analyzed a white Portland cement, which has been hydrated for 11½ years and stored in water in an airtight container. The ^{27}Al NMR spectrum of this matured, hydrated cement (Figure 10) shows resonances from Al(IV), Al(V) and Al(VI) from the C-(A)-S-H phase along with two additional resonances from the AFt (ettringite, 13.2 ppm) and AFm (10.5 ppm) phases. Spectral integration combined with simulations (Figure S6) of the octahedral region of the spectra (using the Czjzek model[73]) give the relative intensities of 18.4% - Al(IV), 4.8% - Al(V) and 36.8% - Al(VI) for the C-(A)-S-H phase and 40.0% for the secondary AFt and AFm phases. Thus, the fraction of octahedral Al in the C-(A)-S-H phase is nearly twice the amount of Al(IV), which supports the atomistic calculations by Kunhi Mohamed *et al.*[25] that indicated $Q_p^2(1Al_{VI})$ being more stable than $Q_p^2(1Al_{IV})$ sites at high Ca/Si ratio. In the corresponding ^{29}Si NMR spectrum (Figure 10), a clear high-frequency shoulder is observed to the tall Q^1 resonance, reflecting the relative high amount of Al(VI) in the C-(A)-S-H phase. Simulations of the ^{29}Si NMR spectrum, using the above approach where the relative intensities of the $Q_p^2(1Al_{VI})$ and $Q_p^2(1Al_{IV})$ sites follow the Al(VI)/Al(IV) ratio from ^{27}Al NMR is somewhat challenging (Figure S7), considering the high amount of six-fold

coordinated Al in the C-(A)-S-H. However, an acceptable simulation is achieved when the $Q_p^2(1Al_{VI})$ resonance is shifted slightly towards lower frequency (-77.5 ppm) and the linewidth of the peak is increased from 2.1 pm to 3.0 ppm, as employed in the optimized simulation of Figure 10. The simulation corresponds to the parameters, Al_{IV}/Si = 0.036, Al_{IV+VI}/Si = 0.1.08 and $\overline{CL}_{IV+VI}$ = 7.67, where the fraction of four-fold coordinated Al is in very good agreement with Al_{IV}/Si ratios reported for similar white Portland cements after prolonged hydration.[18,58]

In the present analysis, the ^{29}Si sites neighboring a bridging site are observed at -77.0 (or -77.5) ppm for $Q_p^2(1Al_{VI})$, -80.8 ppm for $Q_p^2(1Al_{IV})$ and -84.3 ppm for a Q_{pa}^2 site (*c.f.* Table 1). This implies that a change in coordination state from Al(IV) to Al(VI) would result in a shift of the ^{29}Si resonance to higher frequency of approx. 3.8 (or 3.3) ppm, *i.e.*, a total shift of approx. 7 ppm for a $Q_p^2(1Al_{VI})$ site relative to the Q_{pa}^2 site. This seems to be a significant shift, considering that the changes occur in the third coordination sphere to the Si atom. The -77.0 ppm resonance is relatively close to the Q^1 peak at -78.4 ppm. Thus, one may speculate whether the -77.0 ppm peak alternatively may originate from end-group Q^1 sites with non-bonded $AlO_x(OH)_{6-x}$ units present in their proximity, since Al in such a configuration is expected to have only a minor effect on the ^{29}Si chemical shift. Such an assignment does not necessarily conflict with the observation of the ^{27}Al (5 ppm) and ^{29}Si (-77 ppm) correlation peak in the two-dimensional $\{^{29}Si\}^{27}Al$ refocused dipolar INEPT MAS spectrum by Kunhi Mohamed *et al.*,[25] since their experiment employed a recoupling time that probes Si – Al distances up to 4.33 Å. Moreover, the Al(VI) correlation peak was much weaker than the Al(IV) resonance, despite its much narrower linewidth which reflects its significantly lower ^{27}Al quadrupole coupling (broadening), as compared to the Al(IV) site. This suggests a longer Si – Al distance for Al(VI) as compared to Al(IV), considering the detection of through-space interactions in the dipolar-based 2D correlation experiment. The $(SiO)_2Al(OH)_4$ unit in the bridging site (*i.e.*, the $Q_p^2(1Al_{VI})$ assignment) would exhibit two shorter and four longer Al-O bonds, which is expected to result is a less symmetrical electronic environment. This is also indicated by the DFT calculated ^{27}Al quadrupole coupling constants for these sites in their modelled C-(A)-S-H structures,[25] which range from 2.5 to 8.1 MHz (average 5.3 MHz) for the energetically stable $(SiO)_2Al(OH)_4$ units. The experimental value is somewhat lower (approx. 1.2 MHz),[21] which indicates a more symmetrical electronic environment of the 5.0 ppm Al site. $AlO_x(OH)_{6-x}$ moieties in close proximity to end-groups of the silicate chains will be less stable than $(SiO)_2Al(OH)_4$ units anchored to the silicate framework. This may explain the lower thermal stability of these sites upon thermal treatment[21] and the generally observed invariance in ^{27}Al NMR line shape (quadrupolar broadening) of the 5.0 ppm resonance for C-(A)-S-H phases

with different Ca/Si ratios. Non-bonded octahedral Al sites of the $AlO_x(OH)_{6-x}$ type have been reported in a DNP-enhanced ^{29}Si – ^{27}Al NMR and first-principles calculation study of aluminum supported on silica and of silicon species on alumina surfaces.[74] Two-dimensional {^{29}Si}-^{27}Al scalar- and dipolar-refocused INEPT experiments were used to distinguish Al – Si correlations via bridging oxygens and non-bonded units, respectively. These spectra clearly showed direct bonding between tetrahedral aluminum and the SiO_4 sites in both types of experiments but only weak interactions between octahedral Al and Si in the dipolar-driven spectra, which were ascribed to non-bonded AlO_6 units being present in close proximity to the Si sites.[74]

The ^{29}Si NMR spectra in the present work can all be simulated using the approach where the -77 ppm resonance is assigned to a $Q_p^2(1Al_{VI})$ site, using intensity ratios for Al(VI) and Al(IV) from ^{27}Al NMR. Thus, this assignment, proposed by Kunhi Mohamed *et al*.[25], is adapted in the present work (e.g. as illustrated in Figures 9 and 10 and corresponding to the data in Tables 5, S1 and S2).

^{27}Al NMR resonances from Al(IV) associated with C-(A)-S-H. The ^{27}Al NMR spectra in Figures 1 and 6 indicate the presence of different Al(IV) sites from aluminum in the bridging sites of the silicate chains. This may reflect changes in coordination geometries and local environments in the interlayer of the C-(A)-S-H structure for different Ca/Si ratios (*e.g*., effects from Na^+ and Ca^{2+} ions, OH^- groups and water molecules). This is further examined by comparison of very high field ^{27}Al MAS and $^{27}Al\{^1H\}$ CP/MAS NMR spectra of the C-(A)-S-H samples synthesized with Al/Si_{init} = 0.15 in 1.0 NaOH solutions (three months) and different Ca/Si ratios in Figure 11. These spectra allow identification of three Al(IV) sites with maximum peak intensities at 60, 68, and 76 ppm. The 60 ppm peak is only observed at Ca/Si = 0.6 and 0.8, where it dominates the spectrum for the Ca/Si = 0.6 sample, and it exhibits a smaller $^{27}Al\{^1H\}$ CP efficiency compared to the two other sites. The resonance at 68 ppm, which dominates the Al(IV) region at Ca/Si = 0.8, is observed for all samples and tends to decrease in intensity with increasing Ca content. The Al(IV) resonance at 76 ppm is observed for Ca/Si = 0.8 and higher ratios and shows a similar good $^{27}Al\{^1H\}$ CP efficiency as compared to the site at 68 ppm. This strongly suggests that the Al sites of the 68 and 76 ppm resonances include coordination to hydroxyl groups, in addition to the two Al-O-Si bonds, whereas the significant change in ^{27}Al chemical shift may reflect different interactions with interlayer Na^+ or Ca^{2+} ions.

To further distinguish the Al(IV) sites, ^{27}Al multiple-quantum (MQ) MAS NMR spectra have been obtained for the Ca/Si = 1.0, Al/Si_{init} = 0.10 sample (1.0 M NaOH, 15 months) at 14.1 and 22.3

T (Figure 12). This experiment removes second-order quadrupolar broadening in the indirectly detected (F1) dimension and clearly resolves the two Al(IV) peaks at 68 and 76 ppm at 14.1 T. However, the isotropic projection of the very high field ^{27}Al MQMAS spectrum indicates the presence of another resonance, situated in between these two peaks by the clear shoulder to the 76 ppm peak. Moreover, the broad lines in both the isotropic and anisotropic dimensions as well as the shape and orientations of the contours show that the individual resonances are associated with dispersion in ^{27}Al chemical shift and quadrupole coupling as expected for less-crystalline structures such as C-(A)-S-H. In the 22.3 T spectrum, the contours are oriented almost in the direction of pure chemical shift (P_Q = 0) and thereby primarily affected by chemical shift dispersion, also considering the inverse proportionality of the second-order quadrupolar interaction with magnetic field. The Al(IV) resonances at 68 and 76 ppm are almost invariant in shift and line broadening up on changes in Ca/Si ratio (Figure 11). Thus, a valuable estimate of their ^{27}Al isotropic chemical shift (δ_{iso}) and quadrupolar product parameter ($P_Q = C_Q(1 + \eta_Q^2/3)^{1/2}$; C_Q being the quadrupole coupling constant and η_Q the associated asymmetry parameter) can be obtained from the centers of gravity of the resonances in the $F1$ (δ_{F1}^{CG}) and $F2$ (δ_{F2}^{CG}) dimensions of the ^{27}Al MQMAS NMR spectra, utilizing the relationships[47,75] (in ppm):

$$\delta_{F1}^{CG} = \frac{-17}{31}\delta_{iso} - \frac{3}{1550}\left(\frac{P_Q}{\nu_L}\right)^2 \cdot 10^6 \quad (11)$$

$$\delta_{F2}^{CG} = \delta_{iso} - \frac{3}{500}\left(\frac{P_Q}{\nu_L}\right)^2 \cdot 10^6 \quad (12)$$

The two sets of δ_{F1}^{CG} and δ_{F2}^{CG} values from the ^{27}Al MQMAS spectra in Figure 12 allow calculation of δ_{iso} and P_Q by linear regression analysis (Figure S8), considering the magnetic field dependence of the expressions in Eqs. (11) and (12). This results in the data given in Table 6, which also includes the center of gravity for the resonance at 60 ppm at low Ca/Si ratio (Figure 11), *i.e.*, the Al_d(IV) site.

Earlier ^{27}Al NMR studies at lower magnetic fields of synthesized C-(A)-S-H samples have shown a clear increase in ^{27}Al peak frequency for Al(IV) with increasing Ca/Si ratio.[17,21,23,28] These Al(IV) peaks are now resolved into four distinct Al(IV) sites by application of the very high magnetic field (22.3 T). Distinct tetrahedral sites for C-(A)-S-H phases at 74, 66, and 58 ppm have been reported by Sun *et al.*[22] from ^{27}Al NMR spectra at 17.5 T. These peak frequencies agree well with the ^{27}Al chemical shifts for Al_a(IV), Al_c(IV) and Al_d(IV) in Table 6, considering that no corrections were made for second-order quadrupolar shifts. The 58 ppm resonance was assigned to a Q_{Al}^3 site, which disagrees with the present study since the corresponding Q_{Si}^3 sites ($\delta(^{29}Si) \sim -92$ ppm)[55,76,77] are absent

in the ^{29}Si NMR spectra. The more prominent peaks a 66 and 74 ppm were assigned to bridging Al tetrahedra charge-balanced by Ca^{2+}, Na^{+} or H^{+} and Al(IV)–O–Al(V) or Al(IV)–O–Al(VI) linkages, respectively.[22] Comparison with the present spectra, the assignment of the latter resonance suffers from the fact the Al_a(IV) peak is observed in the Ca/Si range from 0.8 – 1.4 (Figure 11), where Al(V) and Al(VI) are absent in the spectra corresponding to Ca/Si = 0.8 and 1.0. Moreover, an early ^{27}Al MQMAS study (7.1 T) of synthesized C-(A)-S-H samples have also reported two tetrahedral sites corresponding to the δ_{iso}, P_Q parameters, 76.3 ppm, 3.2 MHz and 63.7 ppm, 2.8 MHz, and assigned to Al substituting for pairing and bridging Si sites, respectively.[78] Both the δ_{iso} and P_Q values are similar to the values reported for the Al_a(IV) and Al_c(IV) sites in Table 6, whereas the assignment of the high-frequency peak to Al(IV) in a pairing site is against the most stable C-(A)-S-H structures, predicted by atomistic modelling of the incorporation of Al in C-(A)-S-H structures.[19,20,25]

Most recently, synthesized C-(A-)S-H samples targeting Ca/Si = 0.80, 0.95, 1.20, and 1.40 for Al/Si = 0.05 and 0.10 have been analyzed by ^{27}Al MAS and MQMAS NMR (11.7 T) by Kangni-Foli.[79] For the low Ca/Si samples (0.80), he observed at single Al(IV) site and estimated the parameters δ_{iso} = 60 ± 5 ppm and C_Q = 3.4 ± 1.3 MHz, which agree well with our data for the Al_d(IV) site (Table 5) and this site being the dominating tetrahedral environment at low Ca/Si ratios (Table S2). At the higher Ca/Si ratios, Kangni-Foli identified two different Al(IV) sites in the MQMAS spectra, and reported the parameters δ_{iso} = 69 ± 3 ppm and C_Q = 3.1 ± 1.2 MHz and δ_{iso} = 76 ± 3 ppm and C_Q = 3.1 ± 1.2 MHz,[79] which are rather similar to the values for the Al_c(IV) and Al_a(VI) sites (Table 5), respectively, although of somewhat lower precision. Kangni-Foli assigned the 69 ppm resonance to a bridging tetrahedral Al site, whereas the Al site at 76 ppm was attributed to Al(IV) incorporated in a pairing site in chain structure. The principal argument for this assignment was the significantly higher chemical shift of the resonance (compared to 60 and 69 ppm for the bridging AlO_4 sites), caused by the changes in geometrical parameters such as bond distances and angles expected for a pairing Al site.[79] However, Kangni-Foli also noted that this assignment is not supported by atomistic simulations which show higher stability for tetrahedral Al substituting bridging sites rather the pairing sites, as mentioned above. In the present work, the Al_a(IV) resonance is the dominating Al site for the C-(A)-S-H phases with Ca/Si ≥ 1.0 (Table S2), providing a major contribution to the ^{29}Si NMR intensity of the $Q_p^2(1Al_{IV})$ site and thereby the Al_{IV}/Si ratios determined from the ^{29}Si NMR spectra. Thus, the assignment of Al_a(IV) to a pairing site would significantly reduce the intensity of the $Q_p^2(1Al_{IV})$ site in the ^{29}Si NMR spectra which would impact the convincing correlations reported in Figures 7 and 8. Moreover, a pairing site would require the presence of

$Q_p^1(1Al_{IV})$ and possibly also $Q_b^2(1Al_{IV})$ sites in the ^{29}Si NMR spectra, which have not been identified in this work. Thus, the present study gives no indications of Al(IV) in pairing sites, in agreement with atomistic modelling studies.[19,20,25]

The relative intensities of the Al_a(IV), Al_c(IV) and Al_d(IV) peaks have estimated from spectral simulations of the ^{27}Al NMR spectra in Figure 11 and are shown as a function of the Ca/Si ratio in Figure 13 with the simulations and intensities given in Figure S9 and Table S3. ^{27}Al MAS NMR spectra of the Ca/Si = 1.0, Al/Si = 0.10 C-(A)-S-H samples synthesized in 0.1, 0.5 and 1.0 M NaOH solutions (Figure S10) clearly reveal that the intensity of the Al_a(IV) peak increases with increasing NaOH concentration, which strongly suggests that the Al_a(IV) site is charge-balanced by one Na^+ in its near vicinity and includes a hydroxyl group, considering its $^{27}Al\{^1H\}$ CP efficiency (Figure 11). Moreover, the higher fraction of Al_a(IV) with increasing Ca/Si ratio is in agreement with an increasing amount of interlayer Na^+ ions with higher Ca/Si ratio (see next section). The intensity variation with Ca/Si ratio (Figure 13) and NaOH concentration (Figure S10) is less pronounced for the Al_c(IV) site, and on this basis it is assigned to an Al(IV) site which is charge-balanced by ½Ca^{2+} ion and H^+ (hydroxyl group), again considering the good $^{27}Al\{^1H\}$ CP efficiency for this site. Finally, the Al_d(IV) site, with poor $^{27}Al\{^1H\}$ CP efficiency, may by charge-balanced solely by interlayer Ca^{2+} ions or by a combination of interlayer Ca^{2+} and Na^+ ions. The latter environment, $(Si\text{-}O)_2$-Al-$(O\text{-}Ca/Na)_2$, may also be present for the low-intensity Al_b(IV) site, as it is observed in between the Al_a(IV) and Al_c(IV) sites, despite no indications on its CP characteristics are available from the present analysis and it is only clearly seen in the very high-field MQMAS NMR spectrum (Figure 12).

Incorporation of alkalis in C-(A)-S-H phases. The principal alkali ions in Portland cements are Na^+ and K^+ ions, which in C-S-H and C-(A)-S-H phases generally can serve as charge compensators either in the interlayer of the C-S-H structure or at the surface of the particles.[32,36,39,80] Charge deficit sites originate mainly from the deprotonation of silanol groups (Si-OH) and the replacement of silicon by aluminum in the bridging sites. In an alkali-free system, calcium plays the role of charge-balance, whereas the C-S-H structure can be partly reorganized when alkali ions are present. The alkali ions can replace the role of calcium for charge-balance, which leaves more Ca available for formation of the principal CaO_2 layers, thereby resulting in shorter silicate chains, as evidenced from ^{29}Si NMR along with investigations of phases present in the aqueous solution.[22,31,48]

In this study, the role of sodium on C-(A)-S-H phases, synthesized in NaOH solutions, is examined by ^{23}Na NMR in a quantitative manner. ^{23}Na MAS NMR spectra of C-(A)-S-H samples

with Al/Si = 0.10, different Ca/Si ratios and cured in 1.0 M NaOH for three months are shown in Figure 14. All spectra are dominated by a broad, featureless centerband resonance in the range -3.8 ppm (Ca/Si = 0.8) to -1.6 ppm (Ca/Si = 1.6), however, an additional low-intensity peak is also observed at roughly 5.5 ppm for samples with Ca/Si of 0.6 and 0.8. The dominating peak at -1.6 to -3.8 ppm is ascribed to outer-sphere hydrated sodium ions ($[Na(H_2O)_x]^+$; $x \leq 6$) based on the similarity in ^{23}Na chemical shift and peak shape with those observed by ^{23}Na NMR for outer-sphere complexes produced from the interaction of 0.1 M NaOH solutions with silica, illite, and kaolinite.[81] However, a more detailed structural assignment will require further experiments than conducted at the present stage.

The quantities of sodium in the C-(A)-S-H samples is estimated by ^{23}Na NMR spin-counting, using weighed samples and the central-transition intensity for pure samples of Na_2CO_3 and Na_2SO_4 as two independent intensity references. The 26 samples with different Ca/Si and Al/Si ratios and cured in different solutions of NaOH have been analyzed by this ^{23}Na NMR approach (Tables S1 and S2). These data are compared in Figure 15 with the quantities of Na derived from a direct method combined with mass-balance calculations as described by L'Hôpital *et al*.[31] A convincing correlation between the Na contents from the two methods is observed, thereby suggesting that both methods can provide reliable values for the Na content in solid C-(A)-S-H samples. Linear correlation of the data in Figure 15 gives the equation

$$Na_{NMR}(wt\%) = (0.93 \pm 0.03)\, Na_{MB}(wt\%) + (0.07 \pm 0.11)\; R^2 = 0.981 \qquad (13)$$

which indicate slightly lower Na contents obtained by ^{23}Na NMR. The reason for this minor discrepancy is presently not clarified.

The Na quantities derived from the ^{23}Na NMR spectra of the C-(A)-S-H samples with Ca/Si = 0.6 – 1.6, Al/Si = 0.10 and cured in 1.0 M NaOH solution for the 3 months (Figure 14) are depicted in Figure 16a and show a strong correlation with the Ca/Si ratio. For the C-(A)-S-H sample with Ca/Si = 0.8, the Na content of 6.5 wt% corresponds to the molar ratio Na/Si = 0.40, assuming the 14-Å tobermorite composition for this sample. This ratio is slightly higher than the alkali/Si ratios determined for similar C-(A)-S-H samples synthesized in 0.1 NaOH solutions from mass balance calculations based on solutions concentrations,[31] which may reflect the 10-fold higher NaOH concentration used for the samples in Figure 16. The decrease in Na content with increasing Ca/Si ratio may reflect the overlapping role of sodium and calcium in both the interlayer and at the surface

of the C-(A)-S-H phase, which leads to a competitive behavior. Thus, the presence of higher aqueous calcium concentrations will reduce the alkali uptake, as evidenced by the ^{23}Na NMR data (Figure 16a) and consistent with previous studies using mass-balance calculations and measurement of the exchangeable cations.[31,39] The quantity of Na for the Ca/Si = 1.6 sample is higher than expected, which is attributed to the presence of portlandite ($Ca(OH)_2$) in the solid sample, as detected by thermogravimetric analysis for the actual sample (data not shown), since the formation of portlandite consumes calcium ions and thereby enhances the uptake of Na^+ ions. Furthermore, the concentration of alkali ions in the synthesis solution has an important impact on the alkali incorporation in C-(A)-S-H. This is illustrated in Figure 16b by a positive relation between the NaOH concentration used in the synthesis and the incorporated amount of sodium for the C-(A)-S-H samples with Ca/Si ratios of 0.8 and 1.0, a trend that is tentatively described by a Langmuir isotherm.

The effect of alkali ions on the Al uptake in C-(A)-S-H. Several studies have considered the adsorption and incorporation of alkali ions in C-(A)-S-H phases[31-36] with focus on the effect of the alkali ions on the uptake of aluminum in the C-(A)-S-H structure. For example, for hydrated Portland cement systems it has been shown that an increasing amount of alkalis in Portland cement promotes the incorporation of Al(IV) in the bridging sites of the silicate structure[32] whereas no clear correlations between alkali concentration and Al uptake were reported in other investigations.[31,82,83] Moreover, other studies have found a decrease in the alkali content in the solid C-(A)-S-H phase with increasing Al/(Si+Al) ratio at a given Ca/(Si+Al) ratio.[22,84] Some of these ambiguities may reflect that more than one mechanism is responsible for the incorporation of alkalis and aluminum and that these processes are also dependent on the composition of the C-(A)-S-H phase. The latter hypothesis is examined in the present work, utilizing that the different C-(A)-S-H phases can roughly be divided into two groups depending on their average chain length on pure silicate tetrahedra ($\overline{\mathbf{CL}}_{Si}$). This separation can also be related to the Ca/Si ratios of the C-(A)-S-H samples, utilizing the well-known relationship between average silicate chain length and Ca/Si ratio.[12,29,48,49] Thus, dimer-based C-(A)-S-H phases correspond to high Ca/Si ratios and those with longer chain lengths reflect C-(A)-S-H phases with lower Ca/Si values. The first group has $\overline{\mathbf{CL}}_{Si}$ close to 3, corresponding to high-Ca/Si C-(A)-S-H phases dominated by silicate dimers, whereas the second group has $\overline{\mathbf{CL}}_{Si}$ in the range 4 – 6, representing phases with longer silicate chains (*e.g.* pentameric and octameric units). The data for this division are given in Tables S1 and S2, which also contain $\overline{\mathbf{CL}}_{Si}$, Al_{IV}/Si and Al_{IV+VI}/Si values and the Na contents determined for the solid phases from ^{23}Na NMR and mass-balance calculations. Using these data,

Figure 17 projects the Na content as a function of the Al(IV)/Si values for the two regimes and shows a clear relationship between these measures for the C-(A)-S-H phases with high Ca/Si ratios dominated by silicate dimers (average $\overline{\mathbf{CL}}_{Si}$ = 2.99) and no apparent correlation for the low-Ca/Si phases with higher $\overline{\mathbf{CL}}_{Si}$ values (average $\overline{\mathbf{CL}}_{Si}$ = 4.79). A distinction between the NaOH concentrations of the synthesis solution (Figure 17a) and the specific Ca/Si ratios (Figure 17b) is also made, which shows that the Na content in the C-(A)-S-H phases increases with increasing incorporation of Al(IV) in the bridging sites for both studied NaOH concentrations for the dimer-based phases. Comparison of the Na contents for fixed Ca/Si ratios reveals also an increase in the Na uptake with increasing Al(IV) substitution levels for the dimer-based phases, as most clearly seen for the samples with Ca/Si = 1.0 and 1.2 (Figure 17b). Thus, the data in Figure 17 indicates that alkali ions (Na^+) play an important role on the Al(IV) uptake at high Ca/Si ratios, possibly for charge-balancing the deficits from Si^{4+} substitution by Al^{3+}. This is in agreement with the interpretation of the ^{27}Al NMR spectra, where the Al_a(IV) site is assigned to Al in a bridging site charge-balanced by Na^+ and including a hydroxyl group based on its increasing intensity with increasing Ca/Si ratio (Figure 13) and sodium content (Figure S10). However, this effect is not observed for the C-(A)-S-H phases with longer chains (low Ca/Si ratio), implying that the Al(IV) uptake is subjected by different mechanisms associated with the local structure of the C-(A)-S-H phase. Moreover, similar plots as depicted in Figure 17 are shown using the Al_{IV+VI}/Si ratios in Figure S11, which indicate increasing scatter between the Na contents and Al_{IV+VI}/Si as compared to the Al_{IV}/Si ratios. This suggests that the alkali ions have less influence on the incorporation of six-fold coordinated Al and thereby mainly affects the uptake of Al(IV) in the bridging sites. Combining the results from Figures 16 and 17 suggests that a higher fraction of alkalis are adsorbed to the C-(A)-S-H surface at low Ca/Si ratios, where an overall higher uptake of Na is observed. However, a clear mechanism, describing the role of alkalis on the incorporation of aluminum in C-(A)-S-H with different compositions is not obtained at the present stage and further studies on this issue are in progress. Moreover, different mechanisms for the alkali uptake is foreseen for C-S-H phases without and with aluminum incorporated, as indicated in on-going ^{23}Na and ^{29}Si NMR studies of synthesized C-S-H and C-(A)-S-H samples.

Finally, the ^{23}Na, ^{27}Al and ^{29}Si NMR studies presented in this work propose somewhat different C-(A)-S-H structures for the synthesized phases with low and high Ca/Si ratio. A sketch of these structures and a summary of the ^{27}Al and ^{29}Si NMR resonance assignments are illustrated in Figure 18.

CONCLUSIONS

Cementitious calcium alumino-silicate hydrate, C-(A)-S-H, samples have been prepared with targeted Ca/Si ratios in the range 0.6 – 1.6, Al/Si ratios of 0.05 - 0.2, and cured in 0.1, 0.5, or 1.0 M NaOH solutions for 3 or 15 months. The samples have been analyzed by ^{29}Si and ^{29}Si{^{1}H} CP/MAS NMR (9.39 T), ^{23}Na MAS NMR (14.09 T) and by ^{27}Al MAS and MQMAS NMR at 14.09 and 22.3 T.

From a determination of the ^{29}Si{^{1}H} CP time constants, the cross-polarization time (T_{SiH}) and the ^{1}H rotating-frame relaxation time ($T_{1\rho}^{H}$), the ^{29}Si NMR resonance at -87 ppm is assigned to a second type of chain pairing site (Q_{pb}^2, Figure 18) rather than a bridging site interacting with a neighboring bridging site via hydrogen bonding (site often denoted as Q_u^2). The Q_{pb}^2 site is proposed to reflect pairing SiO_4 sites in between bridging tetrahedra in octameric or longer silicate chains. The ^{29}Si NMR spectra have been simulated with this assignment and the restriction [$I(Q_{pa}^2)$ + $I(Q_{pb}^2)$]/$I(Q_b^2)$ = 2, imposed by the dreierketten silicate structure in the defect tobermorite model. This has provided measures for the average chain lengths of alumino-silicate and pure silicate tetrahedra along with the Al_{IV}/Si ratio, the latter based on the relative intensity for pairing sites with an aluminum neighbor (*i.e.*, $Q_p^2(1Al_{IV})$). The fractions of aluminum in tetrahedral, five-fold and octahedral coordination, associated with the C-(A)-S-H phases, have been determined from the distinct resonances for these environments in ^{27}Al NMR spectra, allowing an independent determination of the Al/Si ratio when combined with the synthesis composition and concentrations of Si and Al in the filtrates from ion chromatography. Combining these data have revealed a quantitative 1:1 correlation between Al_{IV}/Si from ^{29}Si NMR and the Al(IV)/Si ratio from ^{27}Al NMR, demonstrating that the $Q_p^2(1Al_{IV})$ resonance only reflects coupling to Al in tetrahedral coordination. This relation has been assumed in several ^{29}Si NMR studies of aluminum-substituted C-S-H phases in the past, and it is confirmed by the 1:1 correlation reported here. However, consideration of the sum of Al(IV) and Al(V) in the correlation with the Al_{IV}/Si ratios from ^{29}Si NMR gives nearly the same result. This reflects the generally low fraction of five-fold coordinated Al (below 10%) and the uncertainties associated with the Al_{IV}/Si ratio from ^{29}Si NMR. Thus, it cannot be excluded that five-fold coordinated Al is also present in the bridging sites of the silicate chain structure. A recent theoretical and experimental NMR study has suggested that six-fold Al is also present in the bridging sites of the silicate chain structure, resulting in a $Q_p^2(1Al_{VI})$ resonance a -77 ppm in the ^{29}Si NMR spectra.[25] Indications of this resonance is seen in a ^{29}Si NMR spectrum of a white Portland cement hydrated for 11½ years. Although, this resonance is not clearly resolved in the ^{29}Si NMR spectra of the C-(A)-S-

H samples, it has been included in the simulation approach, using the relative intensities for the Al(IV) and Al(VI) resonances observed by ^{27}Al NMR to constrain the intensity for the a $Q_p^2(1Al_{VI})$ peak. Satisfactory simulations have been achieved by this approach, supporting the results of Kunhi Mohamed *et al*.[25] and providing new measures for the Al_{IV+VI}/Si ratios and average aluminosilicate chains lengths ($\overline{CL}_{IV+VI}$) for the studied C-(A)-S-H phases.

The ^{27}Al MQMAS and MAS NMR spectra obtained at very high magnetic field have shown the presence of at least four distinct Al(IV) sites, which presence and intensity depend on the Ca/Si ratio of the C-(A)-S-H structure. Their ^{27}Al chemical shifts vary from 61 to 76 ppm with a clear change to higher frequency with increasing Ca/Si ratio. These differences are ascribed to interactions with non-bonded Ca^{2+} ions and sodium ions in the interlayer structure of the C-(A)-S-H phase, and an assignment for the three most prominent Al(IV) sites is proposed (Figure 18).

The uptake of alkali ions has been studied quantitatively by ^{23}Na NMR, which reveals that the amount of sodium associated with the C-(A)-S-H phase decreases with increasing Ca/Si ratio. Sodium is either adsorbed to the C-(A)-S-H surface or present in the interlayer regions. At both places competition with Ca^{2+} ions may occur, accounting for the reduction in alkali uptake when the aqueous calcium concentration is increased at higher Ca/Si ratio. The studied C-(A)-S-H samples fall in groups with short average silicate chains ($\overline{CL}_{Si}$ = 2.84 – 3.13) and longer pure silicate chains ($\overline{CL}_{Si}$ = 3.73 – 5.82), roughly corresponding to samples with high and low Ca/Si ratios, respectively. A clear correlation between the Na content and the Al_{IV}/Si ratio from ^{27}Al NMR is observed for the group of samples with low Si values (*i.e*., high-Ca/Si C-(A)-S-H), whereas no relationship is found for the samples with long chain lengths corresponding to low-Ca/Si C-(A)-S-H. Thus, the alkalis may charge-balance the aluminum for silicon substitution in the bridging sites of the C-(A)-S-H samples with high Ca/Si ratio and thereby facilitate the uptake of aluminum. Finally, it is noted that clear relationships between the appearance of the ^{23}Na resonances (line broadening and chemical shift) and the structure/composition of the C-(A)-S-H phases are presently not available. This may reflect the hydrated environment for the Na^+ ions and calls for further ^{23}Na NMR studies of the interaction and uptake of alkali ions in C-S-H and C-(A)-S-H phases.

The present work illustrates that detailed information about the structure and composition of C-(A)-S-H phases can be achieved from ^{23}Na, ^{27}Al and ^{29}Si NMR experiments. These methods may also be applicable to other amorphous systems or minerals where aluminum and silicon are major building blocks. ^{27}Al and ^{29}Si NMR are in general well-established techniques in studies of C-(A)-S-H phases and Portland cement systems, whereas further research is needed for ^{23}Na NMR to bring this approach

to the same information level. This includes studies of the hydration state of sodium in different environments and experiments that attempt to locate the Na^+ ions in the interlayer of the C-(A)-S-H phase or on its surface. In this context, ^{23}Na-^{23}Na and heteronuclear correlation (*e.g.* ^{23}Na – ^{29}Si) NMR experiments may be particularly useful. Finally, it is foreseen that implementation of heteronuclear NMR experiments for ^{27}Al – ^{29}Si distance measurements may provide further details on the exact location of Al in the aluminosilicate chains of C-(A)-S-H and potentially in the vicinity thereof.

ASSOCIATED CONTENT

Supporting Information

Mean chain lengths of pure silicate tetrahedra ($\overline{CL}_{Si}$), Al_{IV}/Si and Al_{IV+VI}/Si ratios and Na contents from ^{23}Na MAS NMR and mass balance calculations for the additional 26 C-(A)-S-H phases studied in this work (Tables S1 and S2); relative ^{27}Al NMR intensities for the different Al(IV) sites for C-(A)-S-H phases with different Ca/Si ratios (Table S3); simulated ^{29}Si NMR spectra for C(A)-S-H samples with Ca/Si = 0.6 – 1.6 (Figure S1); simulated $^{29}Si\{^1H\}$ CP/MAS NMR spectrum (Figure S2); $^{29}Si\{^1H\}$ CP contact-time curves for the Q^0, Q^1 and $Q_p^2(1Al_{IV})$ sites (Figure S3); plot of $(Al_{IV}/Si)_{Si}$ ratio as function of [Al(IV) + Al(VI)]/Si ratio from ^{27}Al NMR (Figure S4); Al_{IV+VI}/Si ratios from ^{29}Si NMR (Eq. (9)) as a function of the [Al(IV) + Al(VI)]/Si ratios from ^{27}Al NMR for 32 different C-(A)-S-H phases (Figure S5); simulation of the octahedral region for the ^{27}Al NMR spectrum of the white Portland cement hydrated for 11½ years (Figure S6); Optimized simulations of the ^{29}Si NMR spectrum for the white Portland cement hydrated for 11½ years using different fixed values for the chemical shift (δ) and linewidth (w) for the $Q_p^2(1Al_{VI})$ resonance (Figure S7); plot of the centers of gravity for the $Al_a(IV)$ and $Al_c(IV)$ resonances observed in the isotropic and anisotropic dimensions of the ^{27}Al MQMAS NMR spectra as function of the magnetic field dependencies (Figure S8); simulated high-field ^{27}Al NMR spectra for C-(A)-S-H samples with different Ca/Si ratio for the determination of the relative intensities for the different Al(IV) sites (Figure S9); ^{27}Al NMR spectra (22.3 T) for the Ca/Si = 1.0 and Al/S_{init} = 0.10 samples cured in solutions with different NaOH concentration (Figure S10); Na contents in C-(A)-S-H samples from ^{23}Na NMR as function of the Al_{IV+VI}/Si ratios (Figure S11).

AUTHOR INFORMATION

Corresponding Author

Jørgen Skibsted − *Department of Chemistry and Interdisciplinary Nanoscience Center (iNANO), Aarhus University, DK-8000C Aarhus C, Denmark*;

orcid.org/ 0000-0003-1534-4466; Phone: +45-2899 2029;

Email: jskib@chem.au.dk; Fax: +45 8619 6199

Authors

Sheng-Yu Yang − *Department of Chemistry and Interdisciplinary Nanoscience Center (iNANO), Aarhus University, DK-8000C Aarhus C, Denmark;* orcid.org/ 0000-0001-7704-6697

Yiru Yan – *Concrete & Asphalt Laboratory, Empa, 8600 Dübendorf, Switzerland;* orcid.org/ 0000-0001-7836-2085

Barbara Lothenbach – *Concrete & Asphalt Laboratory, Empa, 8600 Dübendorf, Switzerland;* orcid.org/ 0000-0002-9020-6488.

Notes

The authors declare no competing financial interest.

ACKNOWLEDGEMENTS

The Danish Council for Independent Research, Technology and Production (No. 7017-00092) and the Swiss National Foundation (No. 200021-169014) are acknowledged for financial support. We thank the Carlsberg-foundation for an equipment grant (No. CF14-0138). Access to the 950 MHz NMR spectrometer at the Danish Center for Ultrahigh-Field NMR Spectroscopy (Ministry of Higher Education and Science Grant AU-2010-612-181) is also acknowledged.

References

1 Schneider, M. The Cement Industry on the Way to a Low-Carbon Future. *Cem. Concr. Res*. **2019**, *124*, 105792.

2 Farfan, J.; Fasihi, M.; Breyer, C. Trends in Global Cement Industry and Opportunities for Long-Term Sustainable CCU Potential for Power-to-X. *J. Clean Prod*. **2019**, *217*, 821–835.

3 Scrivener, K.L.; John, V.M.; Gartner, E.M. Eco-Efficient Cements: Potential Economically Viable Solutions for a Low-CO_2 Cement-Based Materials Industry. *Cem. Concr. Res.* **2018**, *114*, 2–26.

4 Yang, K.-H.; Jung, Y.-B.; Cho, M.-S.; Tae, S.-H. Effect of Supplementary Cementitious Materials on Reduction of CO_2 Emissions from Concrete. *J. Clean. Prod*. **2015**, *103*, 774-783.

5 Lothenbach, B.; Scrivener, K.; Hooton, R.D. Supplementary Cementitious Materials. *Cem. Concr. Res.* **2011**, *41*, 1244–1256.

6 Duxson, P.; Provis, J. L.; Lukey, G. C.; Van Deventer, J. S. J., The Role of Inorganic Polymer Technology in the Development of 'Green Concrete'. *Cem. Concr. Res*. **2007**, *37*, 1590-1597.

7 Shi, C.; Fernandez Jimenez, A.; Palomo, A., New Cements for the 21st Century: The Pursuit of an Alternative to Portland Cement. *Cem. Concr. Res*. **2011**, *41*, 750-763.

8 Skibsted, J.; Snellings, R. Reactivity of Supplementary Cementitious Materials (SCMs) in Cement Blends. *Cem. Concr. Res.* **2019**, *124*, 105799.

9 Taylor, H.F.W. Proposed Structure for Calcium Silicate Hydrate Gel. *J. Am. Ceram. Soc*. **1986**, *69*, 464-467.

10 Cong, X.; Kirkpatrick, R.J. ^{29}Si MAS NMR Study of the Structure of Calcium Silicate Hydrate. *Adv. Cem. Based Mater*. **1996**, *3*, 144-156.

11 Richardson, I.G. Tobermorite/jennite- and Tobermorite/Calcium Hydroxide-based Models for the Structure of C–S–H: Applicability to Hardened Pastes of Tricalcium Silicate, Beta-Dicalcium Silicate, Portland Cement, and Blends of Portland Cement with Blast-Furnace Slag, Metakaolin, or Silica Fume. *Cem. Concr. Res*. **2004**, *34*, 1733–1777.

12 Richardson, I.G. Model Structures for C-(A)-S-H(I). *Acta Cryst*. **2014**, *B70*, 903–923.

13 Merlino, S.; Bonaccorsi, E.; Armbruster, T. Tobermorites: their Real Structure and Order-Disorder (O-D) Character. *Am. Mineral*. **1999**, *84*, 1613 – 1621.

14 Kunhi Mohamed, A.; Parker, S.C.; Bowen, P.; Galmarini, S. An Atomistic Building Block Description of C-S-H – Towards a Realistic C-S-H Model. *Cem. Concr. Res*. **2018**, *107*, 221 – 235.

15 Richardson, I.G.; Brough, A.R.; Brydson, R.; Groves, G.W.; Dobson, C.M. Location of Aluminum in Substituted Calcium Silicate Hydrate (C-S-H) Gels as Determined by ^{29}Si and ^{27}Al NMR and EELS. *J. Amer. Ceram. Soc.* **1993**, *76*, 2285–2288.

16 Richardson, I.G.; Groves, G.W. The Incorporation of Minor and Trace Elements into Calcium Silicate Hydrate (C-S-H) Gel in Hardened Cement Pastes. *Cem. Concr. Res.* **1993**, *23*, 131–138.

17 Faucon, P.; Delagrave, A.; Richet, C.; Marchand, J.M.; Zanni, H. Aluminum Incorporation in Calcium Silicate Hydrates (C−S−H) Depending on Their Ca/Si Ratio. *J. Phys. Chem. B* **1999**, *103*, 7796–7802.

18 Andersen, M.D.; Jakobsen, H.J.; Skibsted, J. Incorporation of Aluminum in the Calcium Silicate Hydrate (C−S−H) of Hydrated Portland Cements: A High-Field ^{27}Al and ^{29}Si MAS NMR Investigation. *Inorg. Chem.* **2003**, *42*, 2280–2287.

19 Qomi, M.J.A.; Ulm, F.-J.; Pellenq, R. J.-M. Evidence on the Dual Nature of Aluminum in the Calcium-Silicate-Hydrates Based on Atomistic Simulations, *J. Am. Ceram. Soc*. **2012**, *95*, 1128-1137.

20 Pegado, L.; Labbez, C.; Churakov, S.Y. Mechanism of Aluminum Incorporation into C-S-H from ab Initio Calculations, *J. Mater. Chem. A*, **2014**, *2*, 3477-3483.

21 Andersen, M.D.; Jakobsen, H.J.; Skibsted, J. A New Aluminium-Hydrate Species in Hydrated Portland Cements Characterized by ^{27}Al and ^{29}Si MAS NMR Spectroscopy. *Cem. Concr. Res.* **2006**, *36*, 3–17.

22 Sun, G. K.; Young, J. F.; Kirkpatrick, R. J. The Role of Al in C–S–H: NMR, XRD, and Compositional Results for Precipitated Samples. *Cem. Concr. Res.* **2006**, *36*, 18–29.

23 Renaudin, G.; Russias, J.; Leroux, F.; Cau-dit-Coumes, C.; Frizon, F. Structural Characterization of C-S-H and C-A-S-H Samples – Part II: Local Environment Investigated by Spectroscopic Analyses. *J. Solid State Chem.* **2009**, *182*, 3320–3329.

24 Pardal, X.; Brunet, F.; Charpentier, T.; Pochard, I.; Nonat, A. ^{27}Al and ^{29}Si Solid-State NMR Characterization of Calcium Aluminosilicate Hydrate, *Inorg. Chem*. **2012**, *51*, 1827 – 1836.

25 Kunhi Mohamed, A.; Moutzouri, P.; Berruyer, P.; Walder, B.J.; Siramanont, J.; Harris, M.; Negroni, M.; Galmarini, S.C.; Parker, S.C.; Scrivener, K.L. *et al*. P. The Atomic-Level Structure of Cementitious Calcium Aluminate Silicate Hydrate. *J. Am. Chem. Soc.* **2020**, *142*, 11060 – 11071.

26 Pardal, X.; Pochard, I.; Nonat, A. Experimental Study of Si – Al Substitution in Calcium-Silicate-Hydrate (C-S-H) Prepared under Equilibrium Conditions. *Cem. Concr. Res*. **2009**, *39*, 637 – 643.

27 L'Hôpital, E.; Lothenbach, B.; Le Saoût, G.; Kulik, D.; Scrivener, K. Incorporation of Aluminium in Calcium-Silicate-Hydrates. *Cem. Concr. Res.* **2015**, *75*, 91–103.

28 L'Hôpital, E.; Lothenbach, B.; Kulik, D. A.; Scrivener, K. Influence of Calcium to Silica Ratio on Aluminium Uptake in Calcium Silicate Hydrate. *Cem. Concr. Res.* **2016**, *85*, 111–121.

29 Haas, J.; Nonat, A. From C-S-H to C-A-S-H: Experimental Study and Thermodynamic Modelling. *Cem. Concr. Res*. **2015**, *68,* 124–138.

30 Walker, S.; Sutou, S.; Oda, C.; Mihara, M.; Honda, A. Calcium Silicate Hydrate (C–S–H) Gel Solubility Data and a Discrete Solid Phase Model at 25 °C Based on Two Binary Non-ideal Solid Solutions. *Cem. Concr. Res.* **2016**, *79*, 1–30.

31 L'Hôpital, E.; Lothenbach, B.; Scrivener, K.; Kulik, D. A. Alkali Uptake in Calcium Alumina Silicate Hydrate (C-A-S-H). *Cem. Concr. Res.* **2016**, *85*, 122–136.

32 Skibsted, J.; Andersen, M. D. The Effect of Alkali Ions on the Incorporation of Aluminum in the Calcium Silicate Hydrate (C–S–H) Phase Resulting from Portland Cement Hydration Studied by ^{29}Si MAS NMR. *J. Amer. Ceram. Soc.* **2013**, *96*, 651–656.

33 Özcelik, V.O.; White, C.E. Nanoscale Charge-Balancing Mechanism in Alkali-Substituted Calcium-Silicate-Hydrate Gels. *J. Phys. Chem. Lett*. **2016**, *7*, 5266-5272.

34 Barzgar, S.; Lothenbach, B.; Tarik, M.; Di Giacomo, A.; Ludwig, C. The Effect of Alkali Hydroxide on Al Uptake by Calcium Silicate Hydrates (C-S-H). *J. Colloid Interf. Sci.*, **2020**, *572*, 246–256.

35 Love, C.A.; Richardson, I.G.; Brough, A.R. Composition and Structure of C-S-H in White Portland Cement – 20% Metakaolin Pastes Hydrated at 25 ºC. *Cem. Concr. Res.* **2007**, *37*, 109 – 117.

36 Hong, S.-Y.; Glasser, F. P. Alkali Sorption by C-S-H and C-A-S-H Gels: Part II. Role of Alumina. *Cem. Concr. Res.* **2002**, *32*, 1101–1111.

37 Viallis, H.; Faucon, P.; Petit, J.-C.; Nonat, A. Interaction between Salts (NaCl, CsCl) and Calcium Silicate Hydrates (C−S−H). *J. Phys. Chem. B* **1999**, *103*, 5212–5219.

38 Garg, N.; Özcelik, V.O.; Skibsted, J.; White, C.E. Nanoscale Ordering and Depolymerization of Calcium Silicate Hydrates in Presence of Alkalis. *J. Phys. Chem. C*. **2019**, *123*, 24873-24883.

39 Bernard, E.; Yan, Y.; Lothenbach, B. Cation Exchange Capacity of Calcium Silicate Hydrates (C-S-H). *Cem. Concr. Res.* **2021**, *143*, 106393

40 Walkley, B.; Rees, G.J. Nicolas, R.S.; van Deventer, J.S.J.; Hanna, J.V.; Provis, J.L. New Structural Model of Hydrous Sodium Aluminosilicate Gels and the Role of Charge-Balancing Extra-Framework Al. *J. Phys. Chem. C* **2018**, *122*, 5673 – 5685.

41 Walkley, B.; Page, S.L.; Rees, G.J.; Provis, J.L.; Hanna, J.V. Nanostructure of CaO-(Na_2O)-Al_2O_3-SiO_2-H_2O Gels Revealed by Multinuclear Solid-State Magic Angle Spinning and Multiple Quantum Magic Angle Spinning Nuclear Magnetic Resonance Spectroscopy. *J. Phys. Chem. C* **2020**, *124*, 1681 - 1694.

42 Skibsted, J.; Hjorth, J. Jakobsen, H.J. Correlation Between ^{29}Si NMR Chemical Shifts and Mean Si-O Bond Lengths for Calcium Silicates. *Chem. Phys. Lett*. **1990**, *172*, 279-283.

43 Massiot, D.; Fayon, F.; Capron, M.; King, I.; Calvé, S. L.; Alonso, B.; Durand, J.-O.; Bujoli, B.; Gan, Z.; Hoatson, G. Modelling One- and Two-Dimensional Solid-State NMR Spectra. *Magn. Reson. Chem.* **2002**, *40*, 70–76.

44 Samoson, A.; Lippmaa, E. Excitation Phenomena and Line Intensities in High-Resolution NMR Powder Spectra of Half-Integer Quadrupolar Nuclei. *Phys. Rev. B* **1983**, *28*, 6567–6570.

45 Amoureux, J.-P.; Fernandez, C.; Steuernagel, S. Z-filtering in MQMAS NMR. *J. Magn. Reson. Ser. A* **1996**, *123*, 116- 118.

46 Amoureux, J.-P.; Fernandez, C.; Frydman, L. Optimized Multiple-Quantum Magic-Angle Spinning NMR Experiments on Half-Integer Quadrupoles. *Chem. Phys. Lett.* **1996**, *259*, 347–355.

47 Massiot, D.; Touzo, B.; Trumeau, D.; Coutures, J. P.; Virlet, J.; Florian, P.; Grandinetti, P. J. Two-Dimensional Magic-Angle Spinning Isotropic Reconstruction Sequences for Quadrupolar Nuclei. *Solid State Nucl. Magn. Reson.* **1996**, *6*, 73–83.

48 Chen, J.J.; Thomas, J.J.; Taylor, H.F.W.; Jennings, H.M. Solubility and Structure of Calcium Silicate Hydrate, *Cem. Concr. Res*. **2004**, *34*, 1499–1519.

49 Sevelsted, T. F.; Skibsted, J. Carbonation of C-S-H and C-A-S-H Samples Studied by ^{13}C, ^{27}Al and ^{29}Si MAS NMR Spectroscopy. *Cem. Concr. Res.* **2015**, *71*, 56–65.

50 Kwan, S.; LaRosa, J.; Grutzeck, M.W. ^{29}Si and ^{27}Al MAS NMR Study of Strätlingite, *J. Am. Ceram. Soc.*, **1995**, *78*, 1921–1926.

51 Dai, Z.; Tran, T. T.; Skibsted, J. Aluminum Incorporation in the C-S-H Phase of White Portland Cement–Metakaolin Blends Studied by ^{27}Al and ^{29}Si MAS NMR Spectroscopy. *J. Am. Ceram. Soc.* **2014***, 97*, 2662–2671.

52 Skibsted, J.; Henderson, E.; Jakobsen, H. J. Characterization of Calcium Aluminate Phases in Cements by ^{27}Al MAS NMR Spectroscopy. *Inorg. Chem.* **1993**, *32*, 1013–1027.

53 Mercury, J.M.R.; Pena, P.; De Aza, A.H.; Turrillas, X.; Sobrados, I. Sanz, J. Solid-state ^{27}Al and ^{29}Si NMR Investigations on Si-Substituted Hydrogarnets, *Acta Mater*. **2007**, *55*, 1183–1191.

54 Faucon, P.; Charpentier, T.; Bertrandie, D.; Nonat, A.; Virlet, J.; Petit, J. Characterization of Calcium Aluminate Hydrates and Related Hydrates of Cement Pastes by ^{27}Al MQ-MAS NMR, *Inorg. Chem.* **1998**, *37*, 3726–3733.

55 Myers, R. J.; L'Hôpital, E.; Provis, J. L.; Lothenbach, B. Effect of Temperature and Aluminium on Calcium (Alumino) Silicate Hydrate Chemistry under Equilibrium Conditions. *Cem. Concr. Res.* **2015**, *68*, 83–93.

56 Richardson, I.G.; Brough, A.R.; Groves, G.W.; Dobson, C.M. The Characterization of Hardened Alkali-Activated Blast-Blast Furnace Slag Pastes and the Nature of the Calcium Silicate Hydrate (C-S-H) Phase. *Cem. Concr. Res*. **1994**, *24*, 813–29.

57 Richardson I.G.; Groves, G.W. The Structure of the Calcium Silicate Hydrate Phases Present in Hardened Pastes of White Portland Cement/Blast-Furnace Slag Blends. *J. Mater. Sci*. **1997**, *32*, 4793–802.

58 Andersen, M. D.; Jakobsen, H. J.; Skibsted, J. Characterization of White Portland Cement Hydration and the C-S-H Structure in the Presence of Sodium Aluminate by ^{27}Al and ^{29}Si MAS NMR Spectroscopy. *Cem. Concr. Res.* **2004**, *34*, 857–868.

59 Sato, H.; Grutzek, M. Effect of Starting Materials on the Synthesis of Tobermorite, *Mater. Res. Soc. Symp. Proc.* **1992**, *245*, 235–240.

60 Klur, I.; Pollet, B.; Virlet, J.; Nonat, A. C-S-H Structure Evolution with Calcium Content by Multinuclear NMR, in: P. Colombet, A.-R. Grimmer, H. Zanni, P. Soozzani (Eds.), *Nuclear Magnetic Resonance Spectroscopy of Cement-Based Materials*, Springer, Berlin 1998, pp. 119–141.

61 Le Saoût, G.; Lécolier, E.; Rivereau, A.; Zanni, H. Chemical Structure of Cement aged at Normal and Elevated Temperatures and Pressures: Part I. Class G oilwell cement, *Cem. Concr. Res.* **2006**, *36*, 71–78.

62 Le Saoût, G.; Lécolier, E.; Rivereau, A.; Zanni, H. Chemical Structures of Cement at Normal and Elevated Temperatures and Pressures, Part II: Low Permeability Class G Oilwell Cement. *Cem. Concr. Res*. **2006**, *36*, 428 – 433.

63 Pines, A.; Gibby, M. G. Waugh, J.S. Proton-Enhanced NMR of Dilute Spins in Solids. *J. Chem. Phys*. **1973**, *59*, 569 - 590.

64 Rodger, S.A.; Groves, G.W.; Clayden, N.J.; Dobson, C. M. Hydration of Tricalcium Silicate Followed by ^{29}Si NMR with Cross-Polarization. *J. Am. Ceram. Soc.* **1988**, *71*, 91 – 96.

65 Bellmann, F.; Damidot, D.; Moser, B.; Skibsted, J. Improved Evidence for the Existence of an Intermediate Phase during Hydration of Tricalcium Silicate. *Cem. Concr. Res*. **2010**, *40*, 875-884.

66 Pustovgar, E.; Sangodkar, R.P.; Andreev, A.S.; Palacios, M.; Chmelka, B.F.; Flatt, R.J.; d'Espinose del Lacaillerie, J.-B. Understanding Silicate Hydration from Quantitative Analyses of Hydrating Tricalcium Silicates. *Nature Comm*. **2016**, *7*, 10952.

67 Mehring M. *Principles of High Resolution NMR in Solids*. 2nd ed. Berlin: Springer-Verlag; 1983.

68 Yannoni, C.S. High-Resolution NMR in Solids: the CPMAS Experiment. *Acc. Chem. Res*. **1982**, *15*, 201 – 208.

69 Cong, X.; Kirkpatrick, R.J. ^{1}H-^{29}Si CPMAS NMR Study of the Structure of Calcium Silicate Hydrate. *Adv. Cem. Res*. **1995**, *27*, 103 – 111.

70 Klur, I.; Jacquinot, J.-F.; Brunet, F.; Charpentier, T.; Virlet, J.; Schneider, C.; Tekely, P. NMR Cross-Polarization when $T_{IS} > T_{1\rho}$; Examples from Silica Gel and Calcium Silicate Hydrates. *J. Phys. Chem. B*, **2000**, *104*, 10162 – 10167.

71 Skibsted, J.; Rasmussen, S.; Herfort, D.; Jakobsen, H.J. ^{29}Si Cross-Polarization Magic-Angle Spinning NMR Spectroscopy – An Efficient Tool for Quantification of Thaumasite in Cement-Based Materials. *Cem. Concr. Comp*. **2003**, *25*, 823 – 829.

72 Walkley, B.; Nicolas, R. S.; Sani, M.-A.; Rees, G.J.; Hanna, J.V.; van Deventer, J. S.J.; Provis, J. L. Phase Evolution of C-(N)-A-S-H/N-A-S-H Gel Blends Investigated via Alkali-Activation of Synthetic Calcium Aluminosilicate Precursors. *Cem. Concr. Res*. **2016**, *89*, 120 – 135.

73 D'Espinose de la Caillerie, J.B.; Fretigny, C.; Massiot, D. MAS NMR Spectra of Quadrupolar Nuclei in Disordered Solids: The Czjzek Model, *J. Magn. Reson*. **2008**, *192*, 244 – 251.

74 Valla, M.; Rossini, A.J.; Caillot, M.; Chizallet, C.; Raybaud, P.; Digne, M.; Chaumonnot, A.; Lesage, A.; Emsley, L.; van Bokhoven, J. A. *et al*. Atomistic Description of the Interface

between Silica and Alumina in Aluminosilicates through Dynamic Nuclear Polarization Surface-Enhanced NMR Spectroscopy and First-Principles Calculations. *J. Am. Chem. Soc*. **2015**, *137*, 10710 – 10719.

75 Samoson, A. Satellite Transition High-Resolution NMR of Quadrupolar Nuclei in Powders. *Chem. Phys. Lett*. **1985**, *119*, 29−32.

76 Gabrovsek, R.; Kurbus, B.; Mueller, D.; Wieker, W. Tobermorite formation in the system CaO, C_3S – SiO_2-Al_2O_3-NaOH-H_2O under Hydrothermal Conditions. *Cem. Concr. Res.* **1993**, *23*, 321-328.

77 Bell, G.M.M.; Bensted, J.; Glasser, F.P.; Lachowski, E.E.; Roberts, D.R.; Taylor, M.J. Study of Calcium Silicate Hydrates by Solid-State High-Resolution ^{29}Si Nuclear Magnetic Resonance, *Adv. Cem. Res*. **1990**, *9*, 23-37.

78 Faucon, P.; Charpentier, T.; Nonat, A.; Petit, J. C. Triple-Quantum Two-Dimensional ^{27}Al Magic Angle Nuclear Magnetic Resonance Study of the Aluminum Incorporation in Calcium Silicate Hydrates. *J. Am. Chem. Soc.* **1998**, *120*, 12075–12082.

79 Kangni-Foli, E. Study of the Kinetics Rates of Low Alkalinity Cementitious Materials Carbonation: Impact on the Microstructure, the Gas Transport and the Mechanical Properties. Université Paris Sciences et Lettres, 2019 (English). NNT: 2019PSLET056, tel-02929257.

80 Renaudin, G.; Russias, J.; Leroux, F.; Frizon, F.; Cau-dit-Coumes, C. Structural Characterization of C-S-H and C-A-S-H Samples—Part I: Long-Range Order Investigated by Rietveld Analyses. *J. Solid State Chem.* **2009**, *182*, 3312–3319.

81 Kim, Y.; James Kirkpatrick, R. ^{23}Na and ^{133}Cs NMR Study of Cation Adsorption on Mineral Surfaces: Local Environments, Dynamics, and Effects of Mixed Cations. *Geochim. Cosmochim. Acta* **1997**, *61*, 5199–5208.

82 Bach, T. T. H.; Chabas, E.; Pochard, I.; Cau Dit Coumes, C.; Haas, J.; Frizon, F.; Nonat, A. Retention of Alkali Ions by Hydrated Low-PH Cements: Mechanism and Na^+/K^+ Selectivity. *Cem. Concr. Res.* **2013**, *51*, 14–21.

83 Chappex, T.; Scrivener, K. Alkali Fixation of C–S–H in Blended Cement Pastes and Its Relation to Alkali Silica Reaction. *Cem. Concr. Res.* **2012**, *42*, 1049–1054.

84 Stade, H. On the Reaction of C-S-H(Di, Poly) with Alkali Hydroxides. *Cem. Concr. Res.* **1989**, *19*, 802–810.

Tables

Table 1. Average ^{29}Si Chemical Shifts ($\bar{\delta}_{Si}$), Chemical-Shift Ranges and Linewidths (*FWHM*) for the ^{29}Si Sites used in the Simulations of the ^{29}Si MAS NMR Spectra for the C-(A)-S-H samples.[a]

Q_i^n site	$\bar{\delta}_{Si}$[b] *(ppm)*	δ_{Si} range *(ppm)*	$\overline{FWHM}$[b] *(ppm)*	*FWHM range (ppm)*
Q^1	-78.4	-78.3 to -78.6	2.41	2.1 – 2.7
$Q_p^2(1Al_{IV})$	-80.8	-80.80 to -80.9	2.10	2.10
Q_b^2	-82.2	-81.8 to -82.6	2.57	2.2 – 2.9
Q_{pa}^2	-84.3	-84.1 to -84.6	2.00	1.9 – 2.1
Q_{pb}^2	-86.7	-86.5 to -86.9	3.00	3.00

[a] Values for simulation of the ^{29}Si NMR spectra for the C-(A)-S-H samples with Ca/Si = 0.6 – 1.6, Al/Si = 0.10 and in 1.0 M NaOH solutions for 3 months. (*c.f.*, Figure 3 and Figure S1).
[b] Averages of the δ_{Si} and *FWHM* values used in the simulations of the six ^{29}Si NMR spectra.

Table 2. Relative Intensities for the Different Silicate Sites from Simulations of ^{29}Si NMR Spectra along with the Al_{IV}/Si Ratios, Average Pure Silicate Chain Lengths ($\overline{CL}_{Si}$) and Alumino-Silicate Chain Lengths ($\overline{CL}_{IV}$) Calculated from these Intensities.

C-(A)-S-H[a] Ca/Si	Q^1 (%)	$Q_p^2(1Al)$ (%)	Q_b^2 (%)	Q_{pa}^2 (%)	Q_{pb}^2 (%)	Al_{IV}/Si[b]	$\overline{CL}_{Si}$[c]	$\overline{CL}_{IV}$[c]
0.6	15.9	17.4	21.7	34.1	10.9	0.087	6.01	13.64
0.8	24.3	16.8	19.8	31.7	7.4	0.084	4.87	8.94
1.0	33.3	15.1	17.4	34.2	-	0.076	4.13	6.46
1.2	50.0	12.6	12.4	25.0	-	0.063	3.19	4.25
1.4	54.4	10.0	12.0	23.6	-	0.050	3.11	3.86
1.6	59.0	14.0	9.0	18.0	-	0.070	2.74	3.63

[a] C-(A)-S-H samples synthesized with Al/Si = 0.10, in 1.0 M NaOH solutions for three months.
[b] Al_{IV}/Si ratios calculated from the Q_i^n intensities using Eq. (3). The estimated error limits are ± 0.010.
[c] Average chain lengths calculated from the Q_i^n intensities using Eqs. (1) and (2). The estimated error limits are ± 0.15.

Table 3. The T_{SiH} and $T_{1\rho}^{H}$ Time Constants Determined from Simulations of the Intensities in Variable-Contact Time $^{29}Si\{^{1}H\}$ CP/MAS NMR Experiments for the C-(A)-S-H Sample Synthesized with Ca/Si = 0.8 and Al/Si = 0.10 in 1.0 M NaOH Solutions for 3 months[a]

	Q^0	Q^1	$Q_p^2(1Al_{IV})$	Q_b^2	Q_{pa}^2	Q_{pb}^2
δ (ppm)[b]	-76.0	-79.0	-81.8	-83.65	-84.20	-87.30
T_{SiH} (ms)	0.22 ± 0.03	0.26 ± 0.04	0.41 ± 0.04	1.05 ± 0.10	0.46 ± 0.04	0.44 ± 0.05
$T_{1\rho}^{H}$ (ms)	10.6 ± 1.1	9.4 ± 1.1	15.0 ± 1.6	59 ± 29	10.1 ± 0.8	11.3 ± 1.3

[a] Determined from three-parameter fits to Eq. (4). The simulated CP curves are shown in Figures 5 and S3.

[b] ^{29}Si chemical shifts used as fixed parameters in the simulations of the $^{29}Si\{^{1}H\}$ CP/MAS NMR spectra (Figure S2).

Table 4. Fractions of Al(IV), Al(V) and Al(VI) from ^{27}Al NMR and Calculated Al_{IV}/Si Ratios of the C-(A)-S-H phases

C-(A)-S-H[a] Ca/Si	Al(IV) (%)	Al(V) (%)	Al(VI) (%)	Al(VI)[b] 2^{nd} phases (%)	Al(VI)[b] 5.0 ppm (%)	Al/Si[c] bulk - IC	Al_{IV}/Si ^{27}Al NMR
0.6	90.1	0	9.9	9.9	0	0.099	0.089
0.8	96.4	0	3.6	3.6	0	0.086	0.083
1.0	81.0	3.5	15.5	6.6	8.9	0.090	0.073
1.2	64.7	7.8	27.5	4.8	22.7	0.095	0.062
1.4	50.4	8.0	41.6	14.6	27.0	0.098	0.049
1.6	70.2	3.5	26.3	14.0	12.3	0.099	0.069

[a] C-(A)-S-H samples synthesized with Al/Si = 0.10, in 1.0 M NaOH solutions for three months.

[b] Fraction of Al(VI) split into the contributions from the secondary phases and Al(VI) associated with the C-(A)-S-H phase (5.0 ppm resonance).

[c] Bulk Al/Si ratio determined from mass balance calculations using the Al and Si concentrations in the filtrates from ion chromatography.

Table 5. Relative Intensities for the Different Silicate Sites from Simulations of ^{29}Si NMR Spectra considering the incorporation of Al(IV) as well as Al(VI) in the Silicate Chain Structure.[a]

C-(A)-S-H[b] Ca/Si	$Q_p^2(1Al_{VI})$[c] (%)	Q^1 (%)	$Q_p^2(1Al_{IV})$ (%)	Q_b^2 (%)	Q_{pa}^2 (%)	Q_{pb}^2 (%)	Al_{IV+VI}/Si	$\overline{CL}_{Si*}$	$\overline{CL}_{IV+VI}$
0.6	-	15.9	17.4	21.7	34.1	10.9	0.087	6.01	13.67
0.8	-	24.3	16.8	19.8	31.7	7.4	0.084	4.87	8.93
1.0	1.6	32.4	14.9	17.2	33.9	-	0.083	4.09	6.68
1.2	4.4	46.1	12.7	12.2	24.6	-	0.086	3.16	4.71
1.4	5.3	49.6	9.9	11.8	23.4	-	0.076	3.09	4.34
1.6	2.4	56.6	14.0	9.0	18.0	-	0.082	2.74	3.82

[a] Al/Si ratios, Al_{IV+VI}/Si, calculated from the Q_i^n intensities using Eq. (7); the estimated error limits are ± 0.010. Average chain lengths, $\overline{CL}_{Si*}$ and $\overline{CL}_{IV+VI}$, calculated from the Q_i^n intensities using Eqs. (8) and (7); the estimated error limits are ± 0.15.

[b] C-(A)-S-H samples synthesized with Al/Si = 0.10, in 1.0 M NaOH solutions for three months.

[c] Results assuming that the -77 ppm resonance is assigned to a $Q_p^2(1Al_{VI})$ site and that the intensities of the $Q_p^2(1Al_{VI})$ and $Q_p^2(1Al_{IV})$ sites follow that intensity ratio of Al(IV) and $Al(VI)_{5ppm}$ observed in the ^{27}Al NMR spectra (Table 4).

Table 6. ^{27}Al Isotropic Chemical Shifts (δ_{iso}) and Quadrupolar Product Parameters (P_Q) for Distinct Tetrahedral Al(IV) Sites from ^{27}Al MQMAS and MAS NMR spectra (14.1 and 22.3 T) of C-(A)-S-H Phases Synthesized with Ca/Si = 0.6 and 1.0 and Al/Si = 0.15.

	δ_{F1}^{CG} (ppm)[a]		δ_{F2}^{CG} (ppm)[a]		δ_{iso} (ppm)	P_Q (MHz)
	14.1 T	22.3 T	14.1 T	22.3 T		
$Al_a(IV)$[b]	-42.31	-42.39	74.55	75.36	76.4 ± 0.2	2.8 ± 0.4
$Al_b(IV)$[b]		-39.44		69.22	70.9 ± 0.4	4.2 ± 0.6
$Al_c(IV)$[b]	-37.50	-37.37	65.73	66.07	67.4 ± 0.3	2.8 ± 0.4
$Al_d(IV)$[c]			60.56	61.28	61.8 ± 0.4	2.2 ± 0.5

[a] Centers of gravity in the isotropic (δ_{F1}^{CG}) and anisotropic (δ_{F2}^{CG}) dimensions of the ^{27}Al MQMAS NMR spectra.

[b] Values determined from the ^{27}Al MQMAS spectra in Figure 12 for the Ca/Si = 1.0 sample.

[c] Value estimated from ^{27}Al MAS NMR spectra of the Ca/Si = 0.6 C-(A)-S-H sample (Figure 11). The center of gravity of the central transition in single-pulse ^{27}Al NMR spectra matches the value for δ_{F2}^{CG} in Eq. (12).

Figures

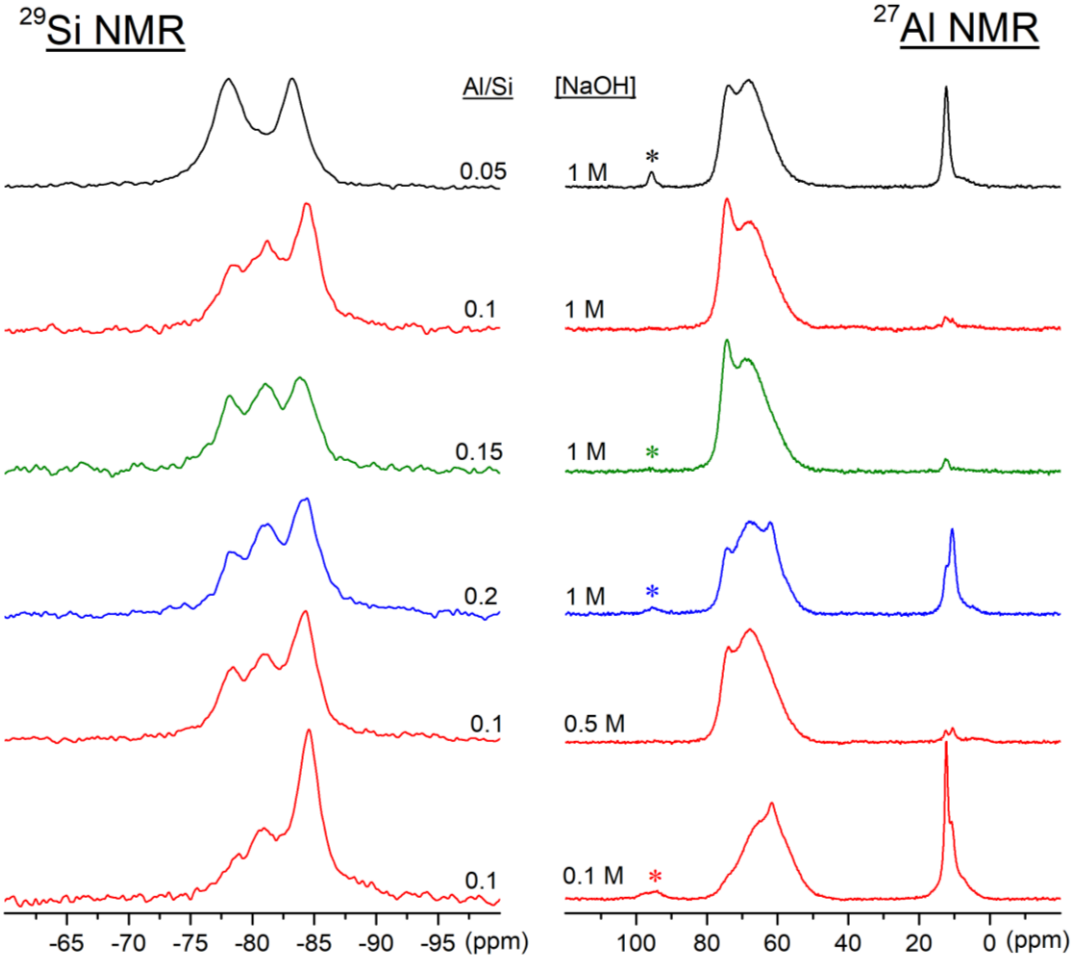

Figure 1. ^{29}Si MAS NMR (9.39 T, ν_R = 10.0 kHz) and ^{27}Al MAS NMR (14.09 T, ν_R = 13.0 kHz) spectra of synthesized C-(A)-S-H samples with Ca/Si = 0.8, Al/Si ratios of 0.05 – 0.20 and cured for three months in 0.1 – 1.0 M NaOH solutions. The asterisks denote spinning sidebands in the ^{27}Al NMR spectra.

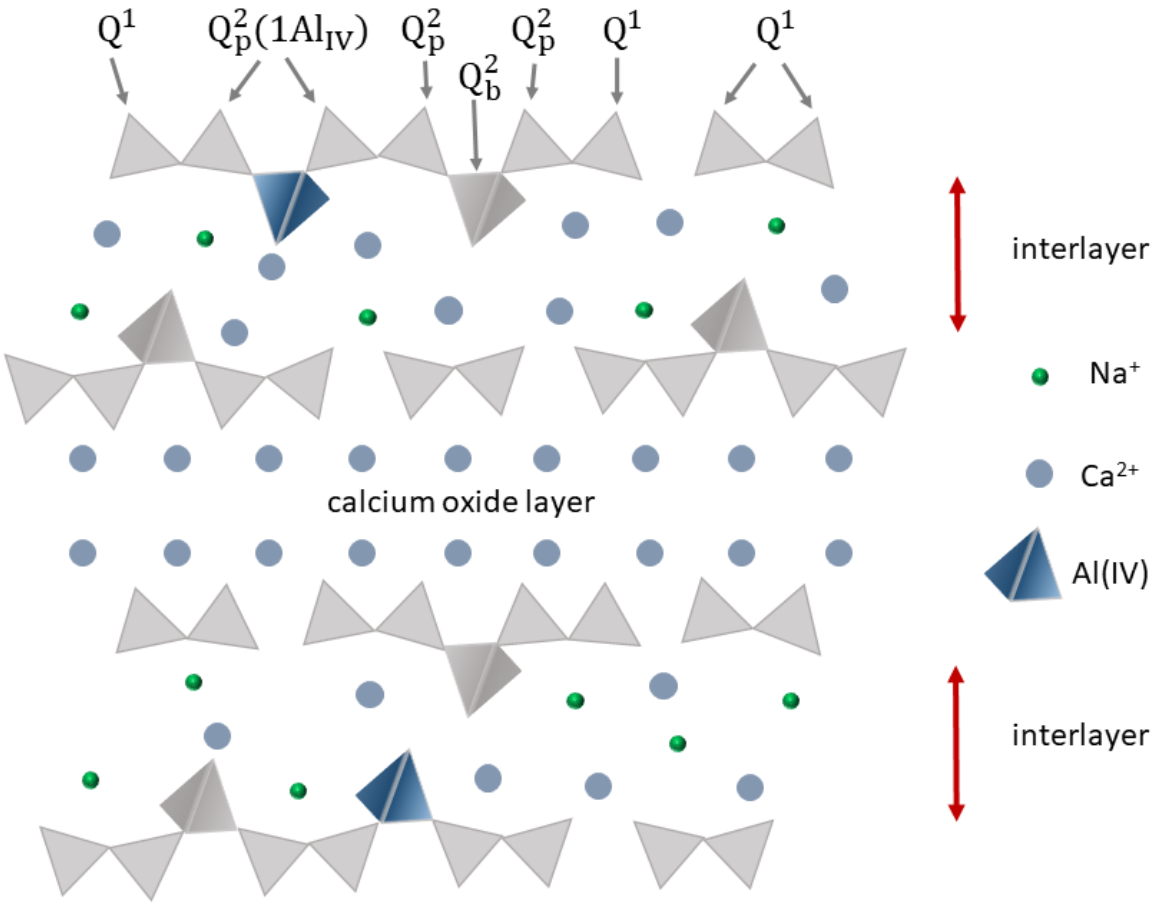

Figure 2. Schematic illustration of the C-(A)-S-H structure based on a defect-tobermorite model and focusing on the local environments for the different silicate species and tetrahedrally coordinated aluminum. The five-fold and octahedrally coordinated Al species associated with the C-(A)-S-H structure, as well as water molecules and hydroxyl groups, are not included in this structural sketch.

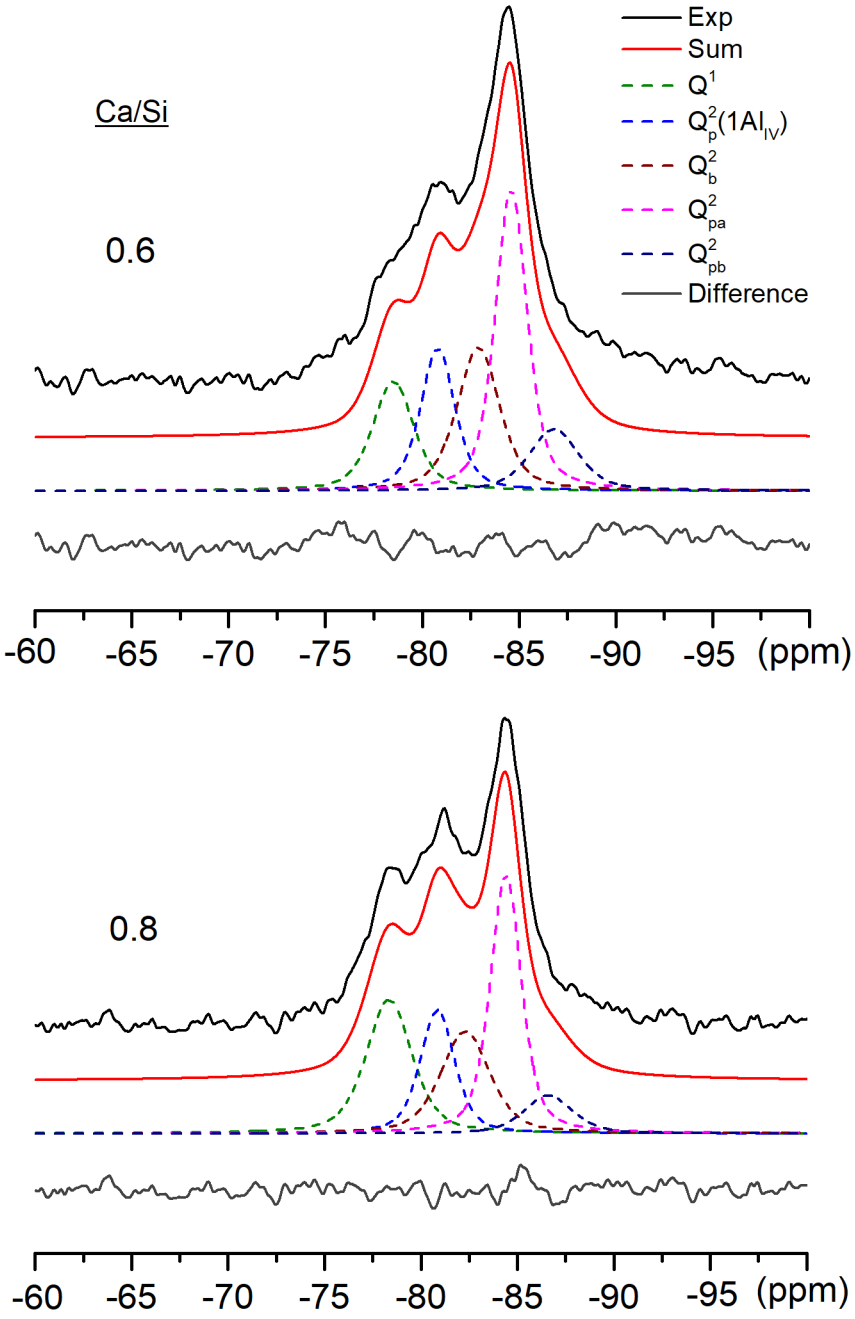

Figure 3. ^{29}Si MAS NMR spectra (9.39 T, ν_R = 10.0 kHz, black lines) of the C-(A)-S-H samples with Ca/Si = 0.6 and 0.8, Al/Si = 0.10, and cured in 1.0 M NaOH solution for three months. Least-squares optimized simulations (red lines) corresponding to the sum of individual peaks shown by the dashed lines and resulting in the parameters listed in Table 2. Difference plots are shown below the simulations of the individual peaks.

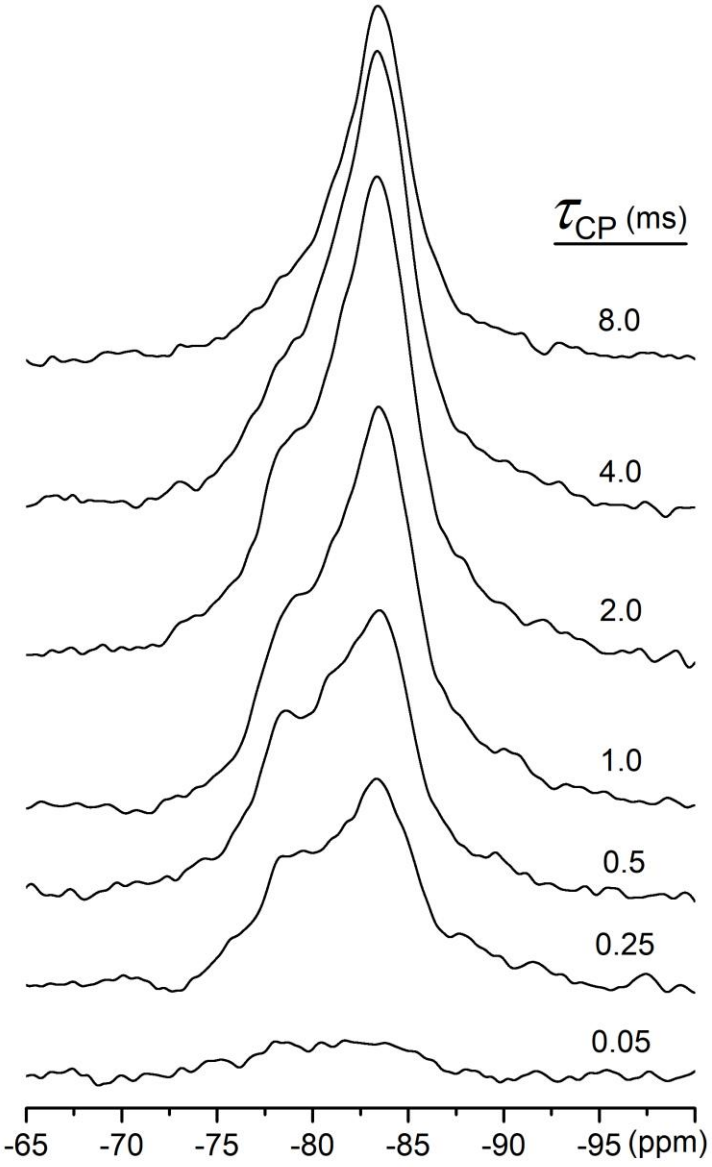

Figure 4. $^{29}Si\{^{1}H\}$ CP/MAS NMR spectra (9.39 T, ν_R = 4.0 kHz) for the C-(A)-S-H sample with Ca/Si = 0.8, Al/Si = 0.10, and cured in 1.0 M NaOH solution for three months, acquired at CP contact times in the range τ_{CP} = 0.05 – 8.0 ms.

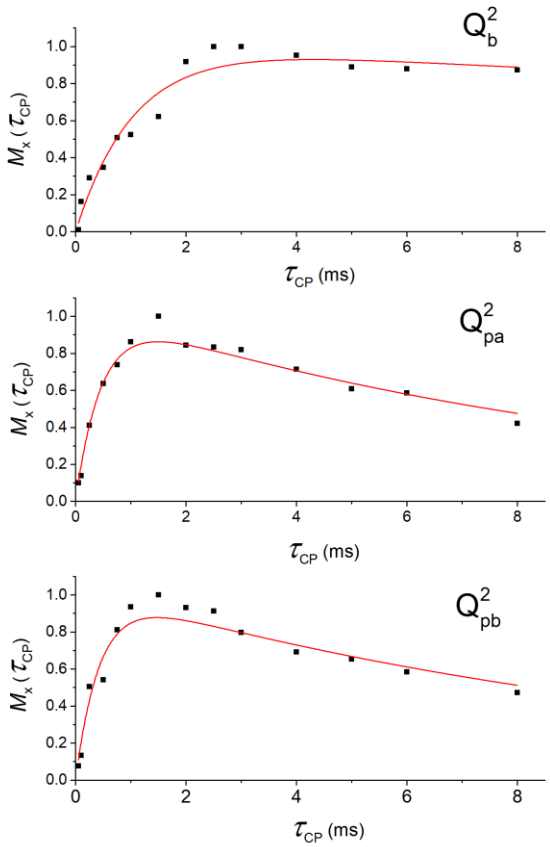

Figure 5. ^{29}Si NMR intensities ($M_x(\tau_{CP})$) as a function of the contact time (τ_{CP}) from simulations of the ^{29}Si{^{1}H} CP/MAS NMR spectra in Figure 4 for the bridging site (Q^2_b) and the pairing site with ^{29}Si chemical shifts of -84.3 ppm (Q^2_{pa}) and -86.7 ppm (Q^2_{pb}). The red curves illustrate the results of least-squares fitting using Eq. (4), corresponding to the values for the T_{SiH} and $T^H_{1\rho}$ time constants listed for the individual Si sites in Table 3.

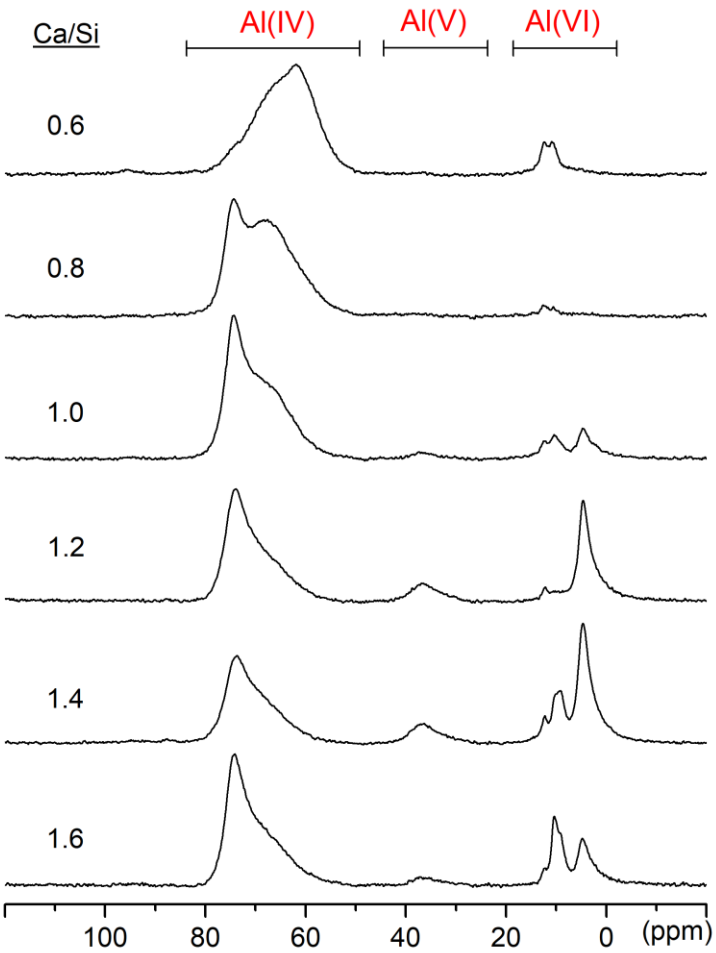

Figure 6. ^{27}Al MAS NMR spectra (14.09 T) for the C-(A)-S-H samples with Ca/Si = 0.6 – 1.6, Al/Si = 0.10 and cured in 1.0 M NaOH solutions for three months. The fraction of aluminum incorporated in the Al(IV), Al(V) and Al(VI) coordination states are determined from these spectra and summarized in Table 4.

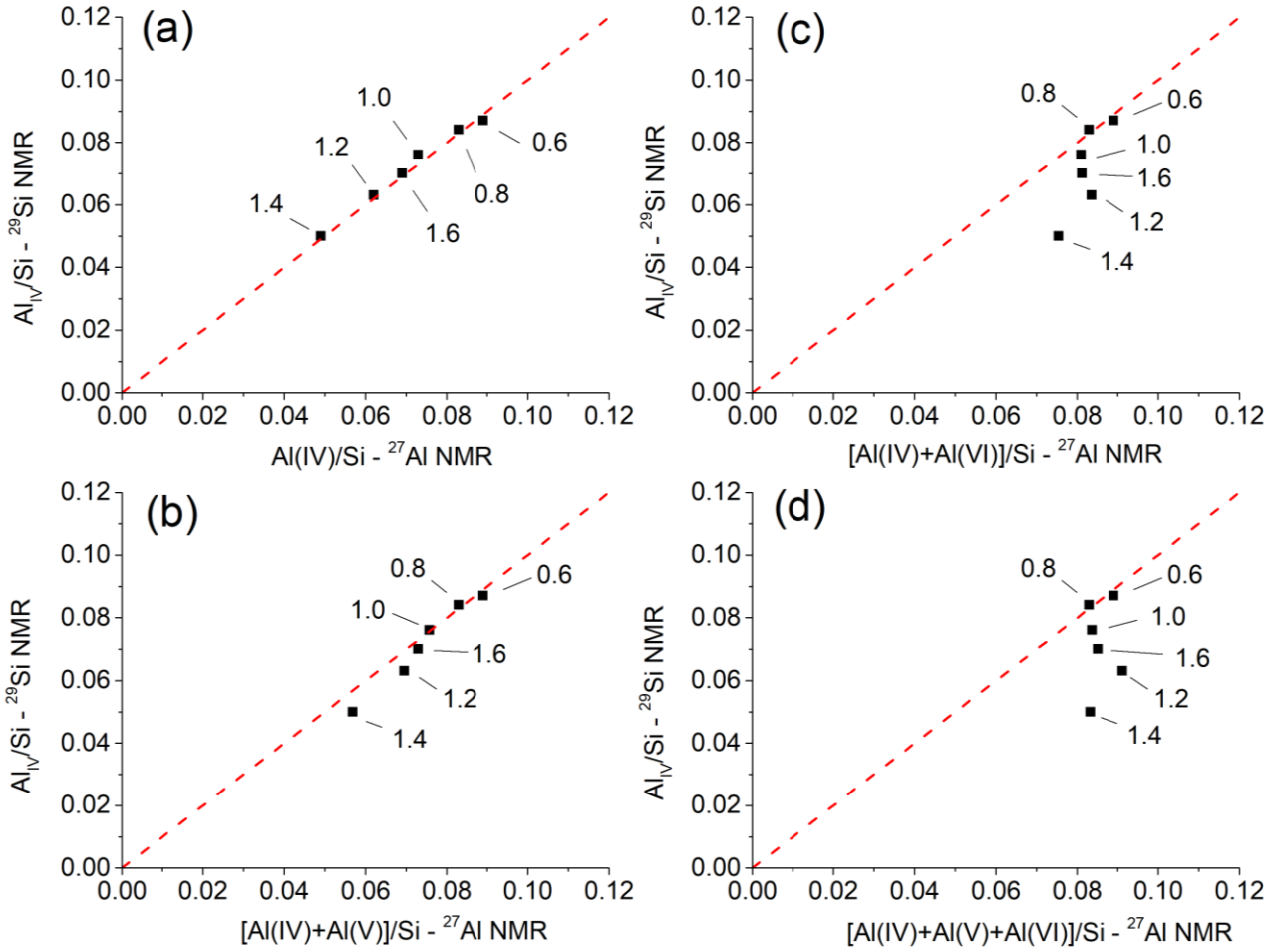

Figure 7. Al/Si ratios from ^{29}Si NMR (Eq. (3)) as a function of the (a) Al(IV)/Si, (b) [Al(IV) + Al(V)]/Si, (c) [Al(IV) + Al(VI)]/Si, and (d) [Al(IV) + Al(V) + Al(VI)]/Si ratios from ^{27}Al NMR for the C-(A)-S-H phases synthesized with an initial ratio Al/Si = 0.10, Ca/Si ratios in the range 0.6 – 1.6 (indicated), and in 1.0 M NaOH solutions for three months. Al(VI) considers only the octahedrally coordinated Al in the 5.0 ppm resonance (*c.f.* Table 4). The red dashed lines indicate 1:1 correlations.

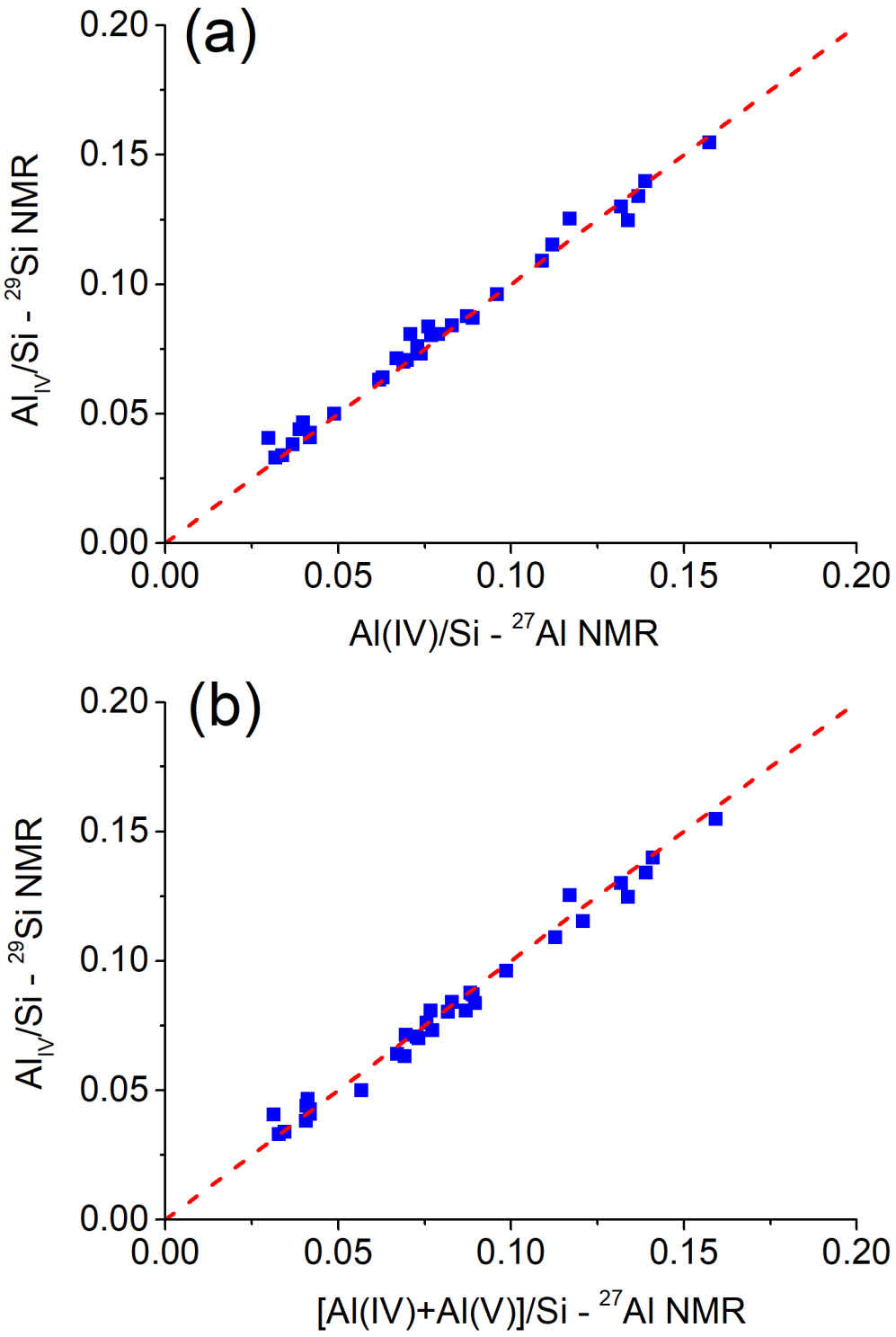

Figure 8. Al/Si ratios from ^{29}Si NMR as a function of the (a) Al(IV)/Si and (b) [Al(IV) + Al(V)]/Si ratios from ^{27}Al NMR for 32 different C-(A)-S-H phases synthesized with Ca/Si ratios in the range 0.6 – 1.6, initial Al/Si ratios 0.05 - 0.20, and in 0.5 or 1.0 M NaOH solutions for three or 15 months. The red dashed lines indicate 1:1 correlations.

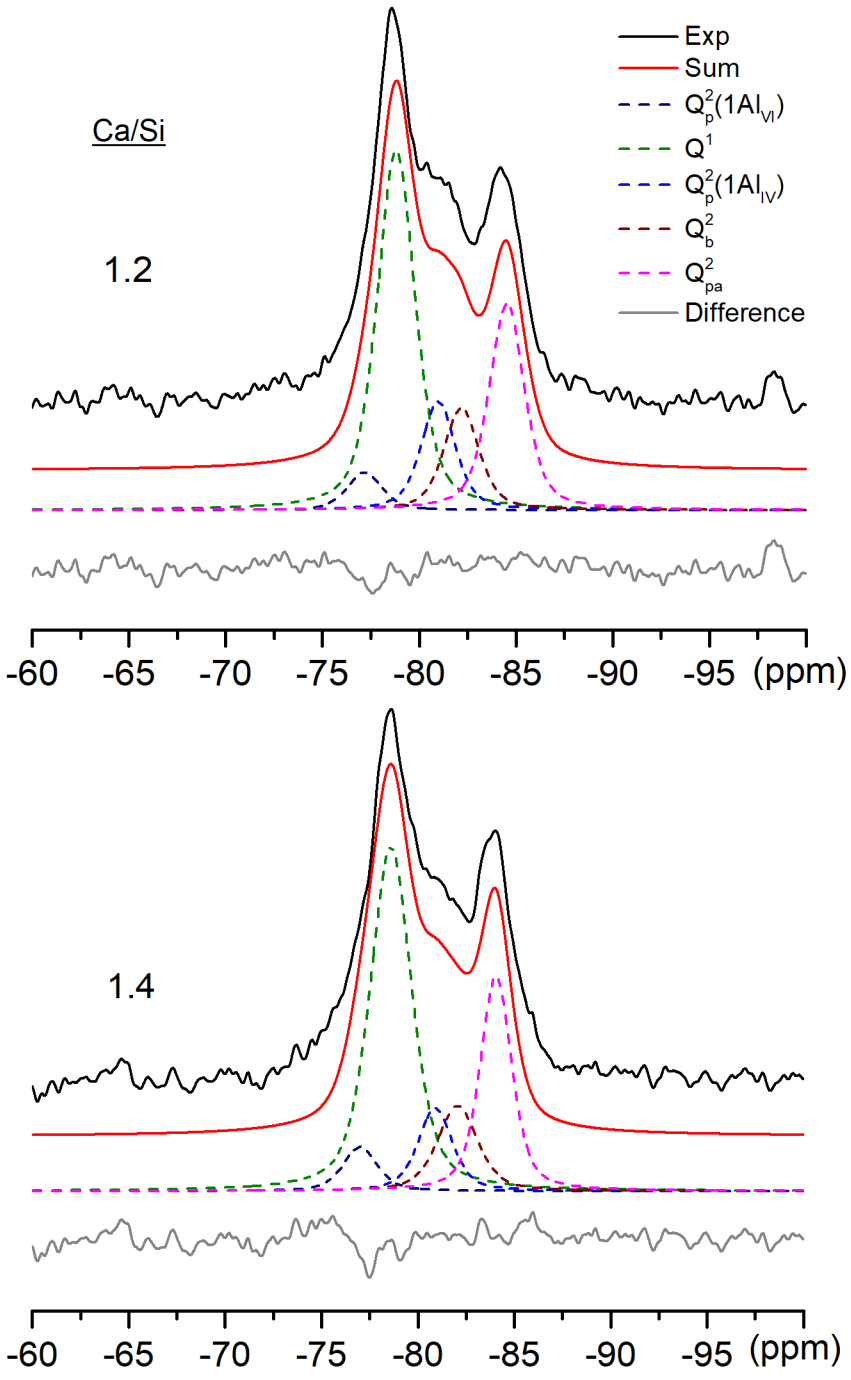

Figure 9. ^{29}Si MAS NMR spectra (9.39 T, ν_R = 10.0 kHz, black lines) of the C-(A)-S-H samples with Ca/Si = 1.2 and 1.4, Al/Si$_{init}$ = 0.10, and cured in 1.0 M NaOH solution for three months. Least-squares simulations (red lines) corresponding to the sum of individual peaks shown by the dashed lines and using restricted intensities for the $Q^2_p(1Al_{VI})$ and $Q^2_p(1Al_{IV})$ sites at -77.0 ppm and -80.8 ppm, respectively, following the corresponding intensities observed by ^{27}Al NMR (Table 4). The intensities for the different silicate sites are listed in Table 5. Difference plots are shown below the simulations of the individual peaks.

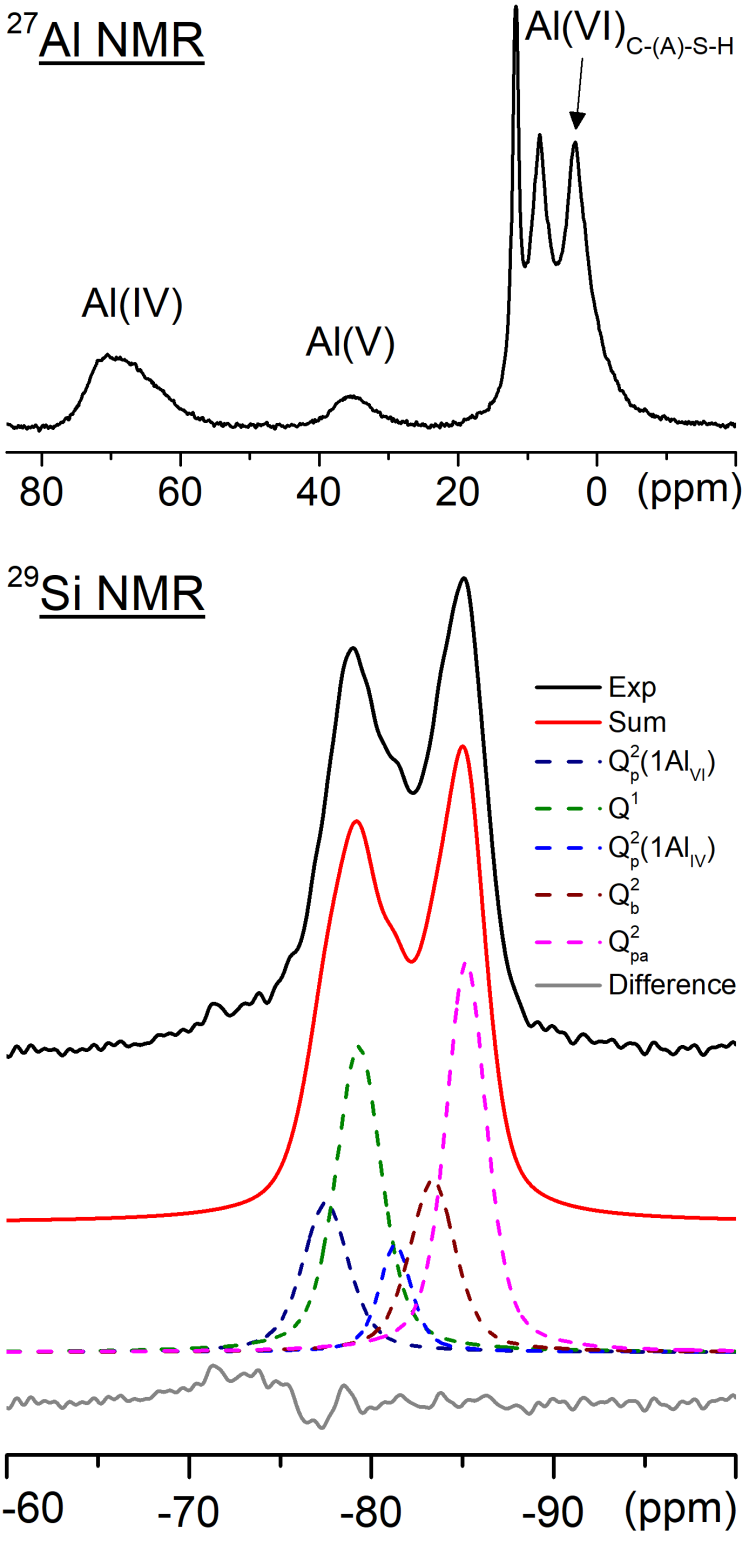

Figure 10. ^{27}Al MAS (14.09 T, ν_R = 13.0 kHz) and ^{29}Si MAS (9.39 T, ν_R = 10.0 kHz) spectra of a white Portland cement hydrated for 11½ years. A simulation of the octahedral region of the ^{27}Al NMR spectrum is shown in Figure S6 and additional simulations of the ^{29}Si NMR spectrum is given in Figure S7.

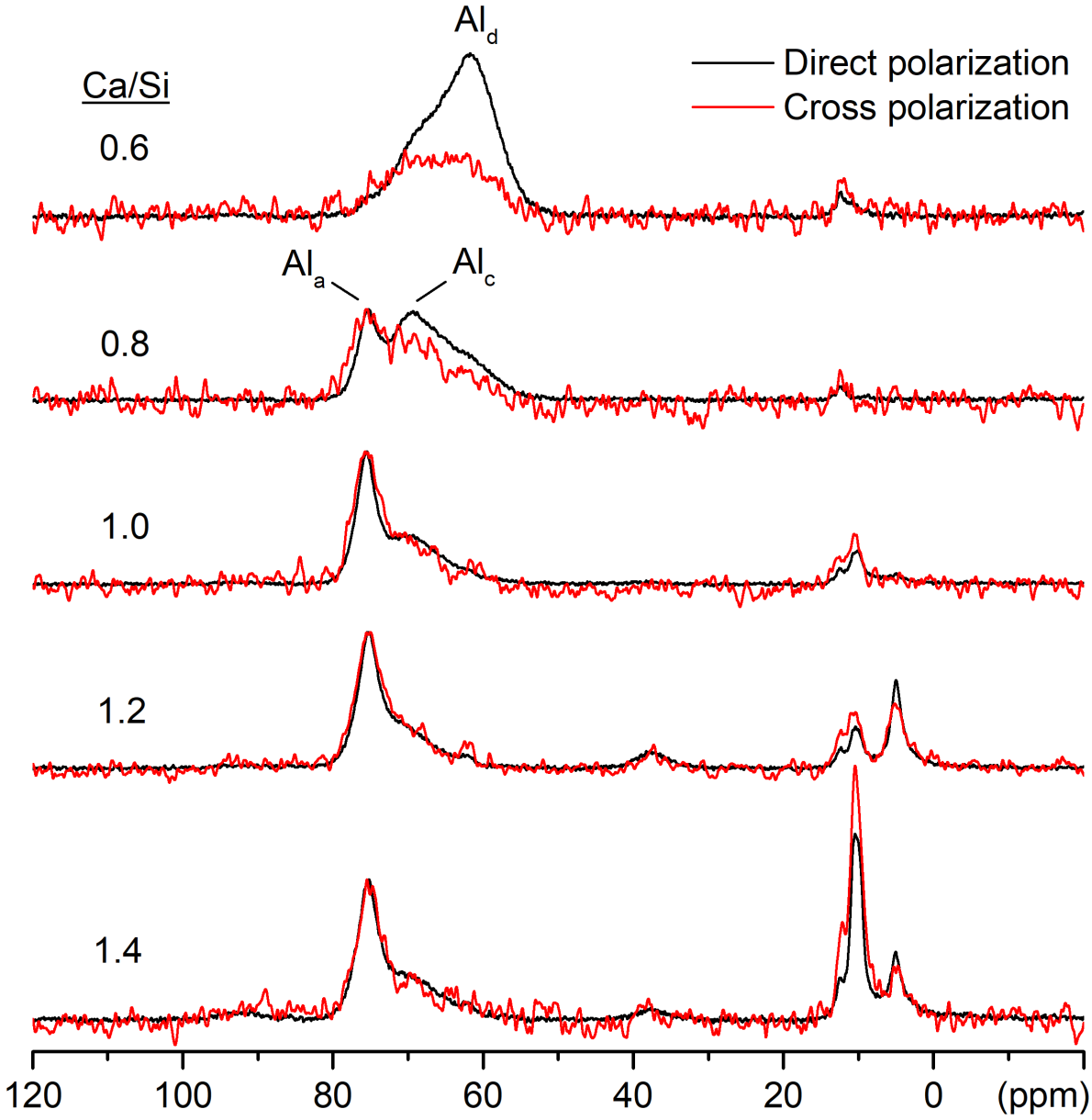

Figure 11. ^{27}Al MAS (black) and ^{27}Al{^{1}H} CP/MAS (red) NMR spectra recorded at 22.3 T (ν_R = 20 kHz) for the C-(A)-S-H samples with Ca/Si = 0.6, 0.8, 1.0, 1.2, 1.4, Al/Si = 0.15 and cured in 1.0 M NaOH for three months. The intensity is normalized based on the resonance at ≈ 75 ppm.

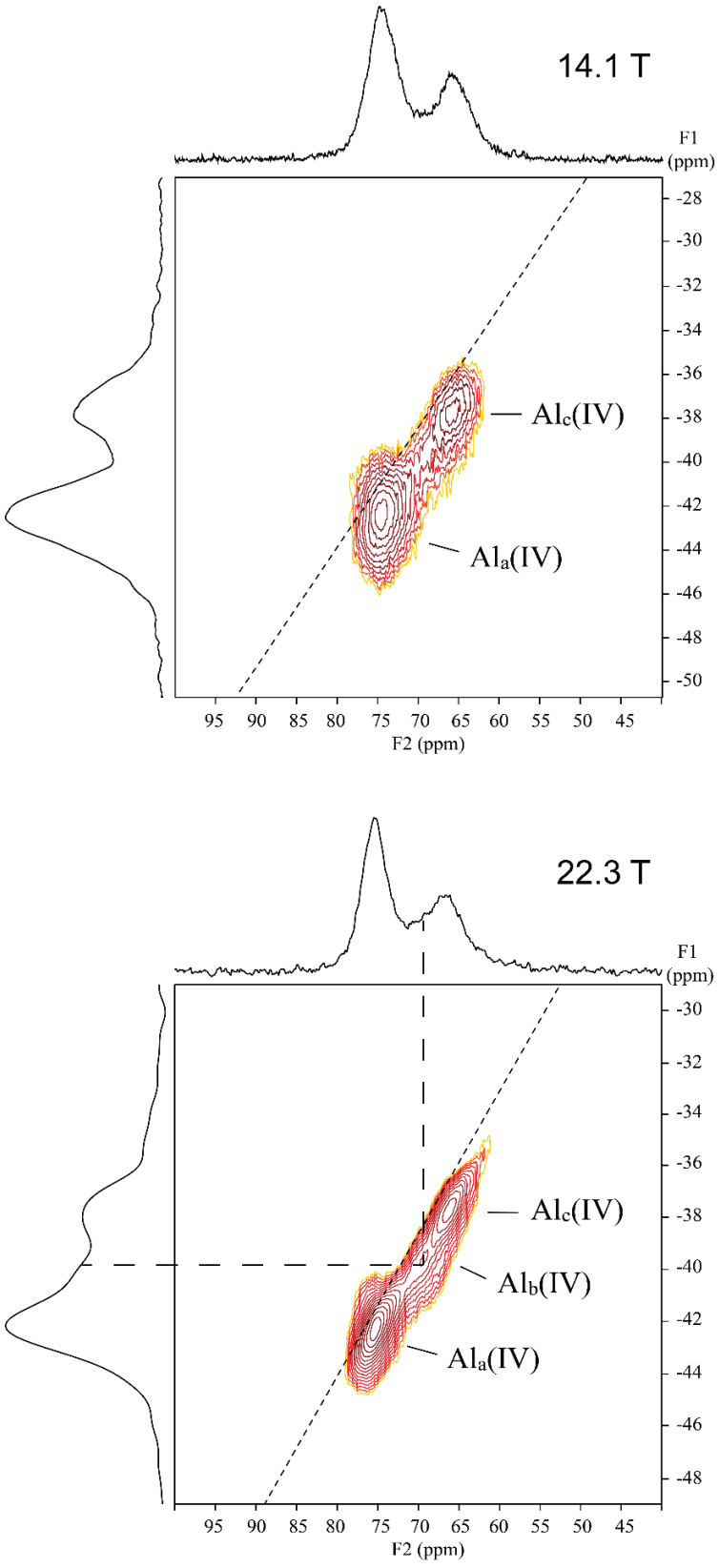

Figure 12. Contour plots of ^{27}Al MQMAS NMR spectra recorded at 14.09 T (ν_R = 13.0 kHz) and 22.3 T (ν_R = 25.0 kHz) with sum projections in both dimensions for the C-(A)-S-H sample with Ca/Si of 1.0, Al/Si = 0.15 and equilibrated in 1.0 M NaOH solution for 15 months. The pure chemical shift direction *(i.e.*, $P_Q = 0$) is indicated by dashed lines.

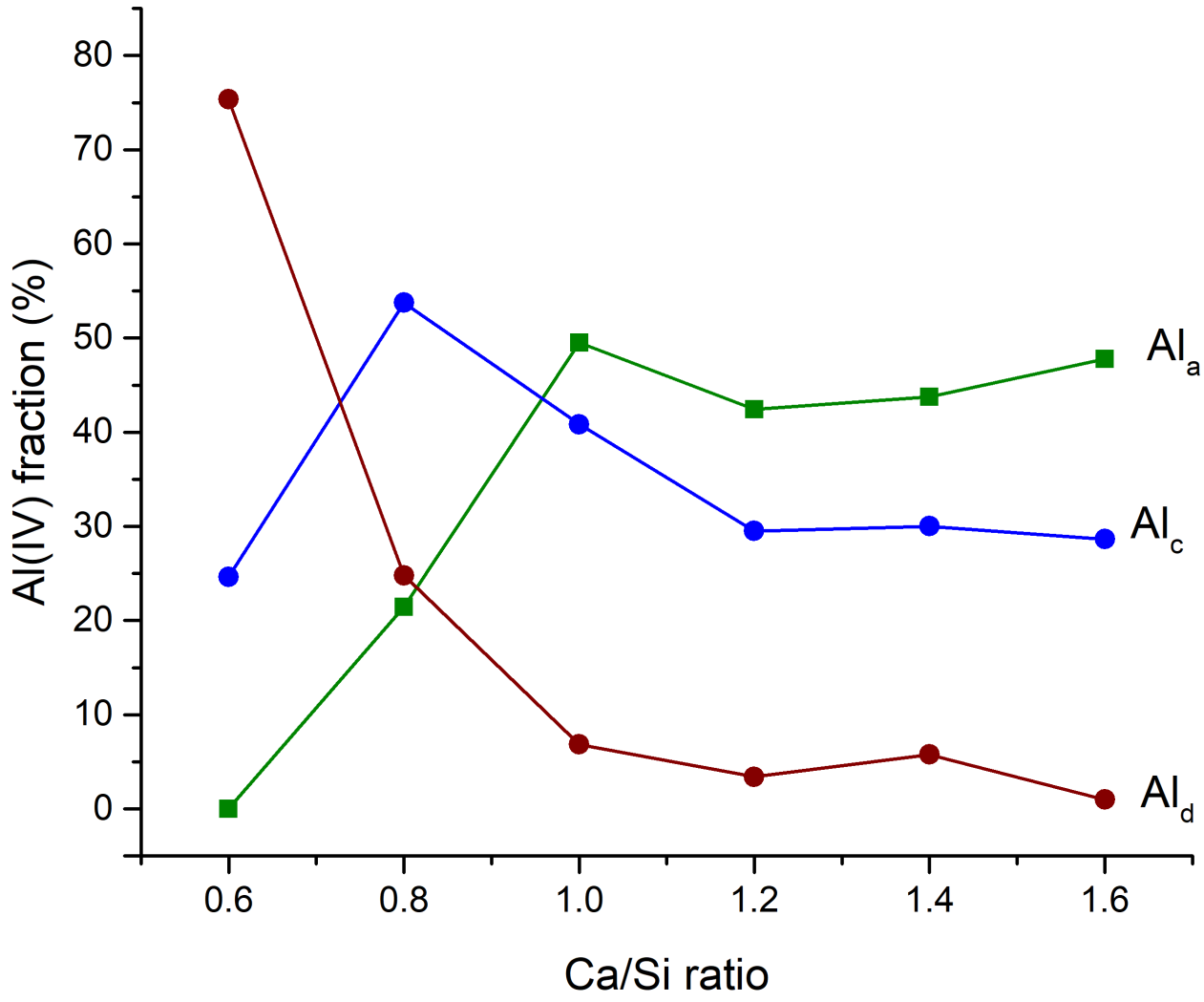

Figure 13. Relative ^{27}Al NMR intensities for the different Al(IV) sites as a function of the Ca/Si ratio for the C-(A)-S-H samples with Al/Si = 0.15 and cured in 1.0 M NaOH for three months. The intensities are derived from simulations of the very high field ^{27}Al NMR spectra in Figure 11 (*c.f.*, Figure S9) and summarized in Table S3.

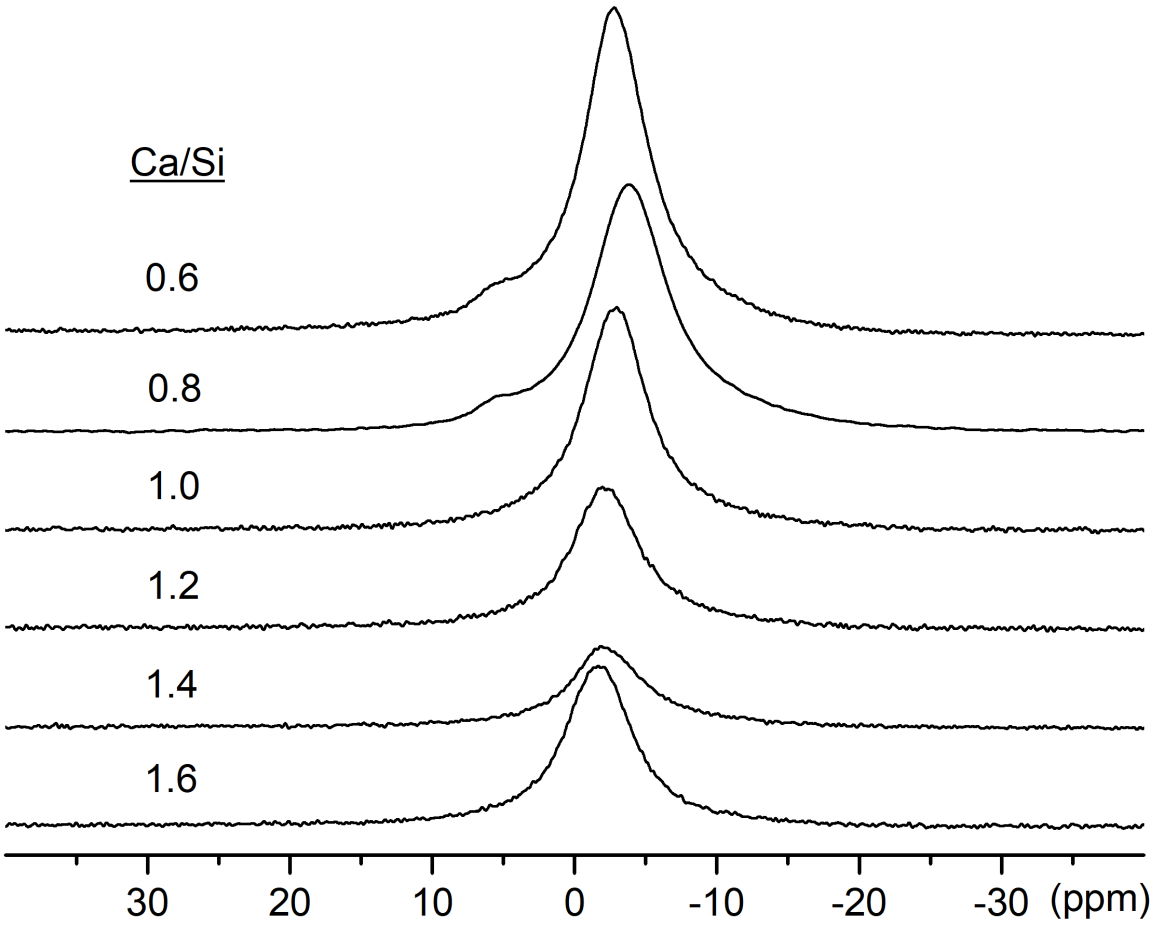

Figure 14. ^{23}Na MAS NMR spectra (14.09 T, ν_R = 12.0 kHz) of the C-(A)-S-H samples with Ca/Si = 0.6 – 1.6, Al/Si = 0.10 and cured in 1.0 M NaOH solution for the 3 months.

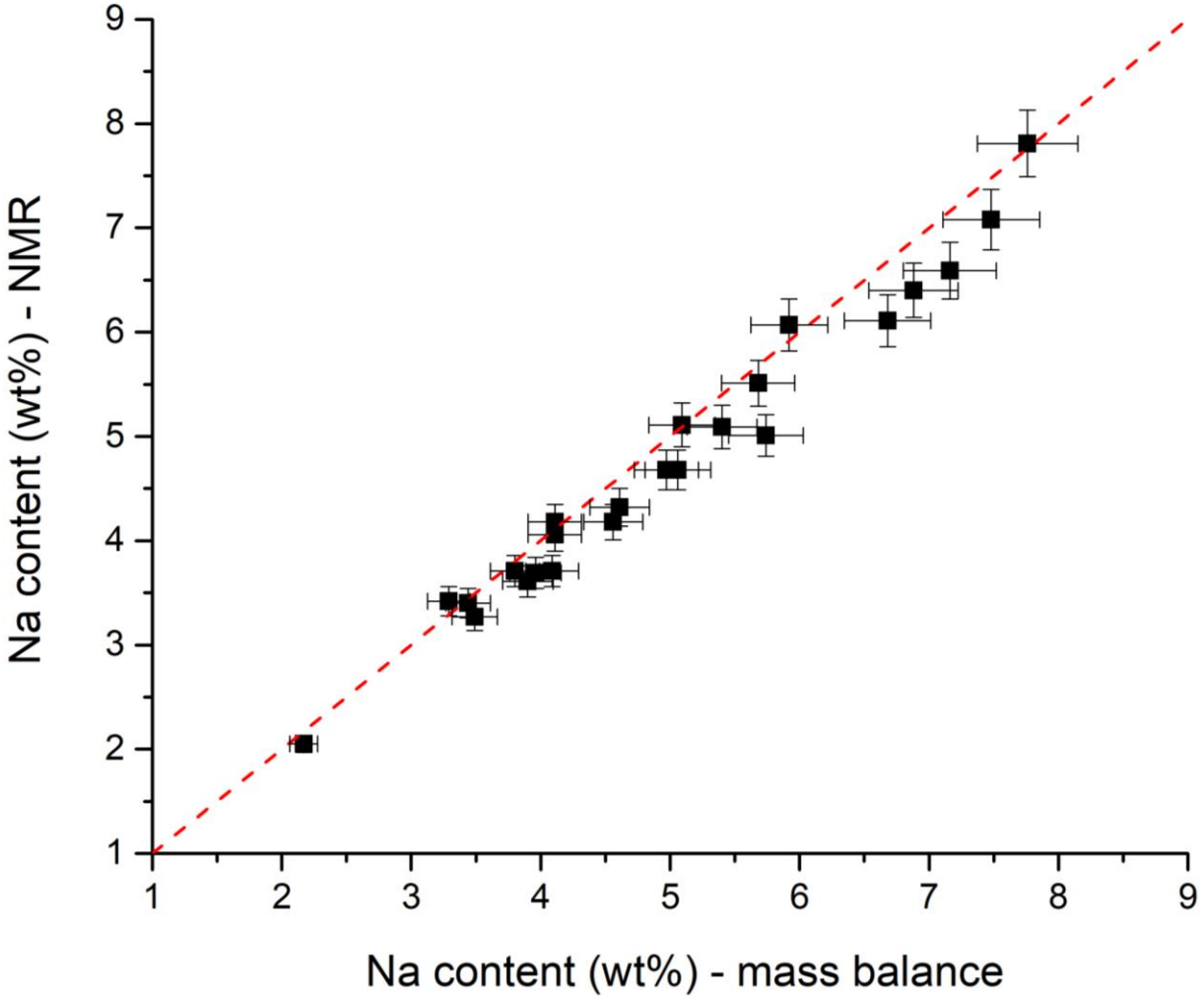

Figure 15. Na contents (wt%) in C-(A)-S-H samples determined by ^{23}Na MAS NMR (spin-counting and central-transition intensities) as function of the quantities of Na in the solid phases derived from ion chromatography analysis of the solutions combined with mass balance calculations. The red dashed line shows the 1:1 correlation. The data from the two methods are summarized in Tables S1 and S2.

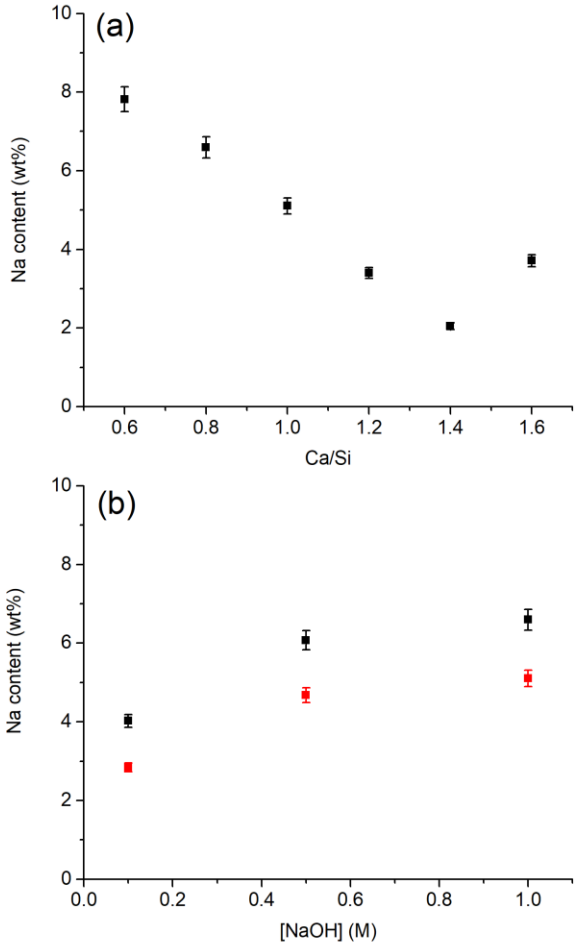

Figure 16. (a) Na contents (wt%) determined by ^{23}Na MAS NMR as a function of the Ca/Si ratio for the C-(A)-S-H samples studied in Figure 14. (b) Na contents (wt%) for the C-(A)-S-H samples prepared with Ca/Si = 0.8 (black squares) or Ca/Si = 1.0 (red squares) and Al/Si = 0.10 in NaOH solutions of different concentrations for three months.

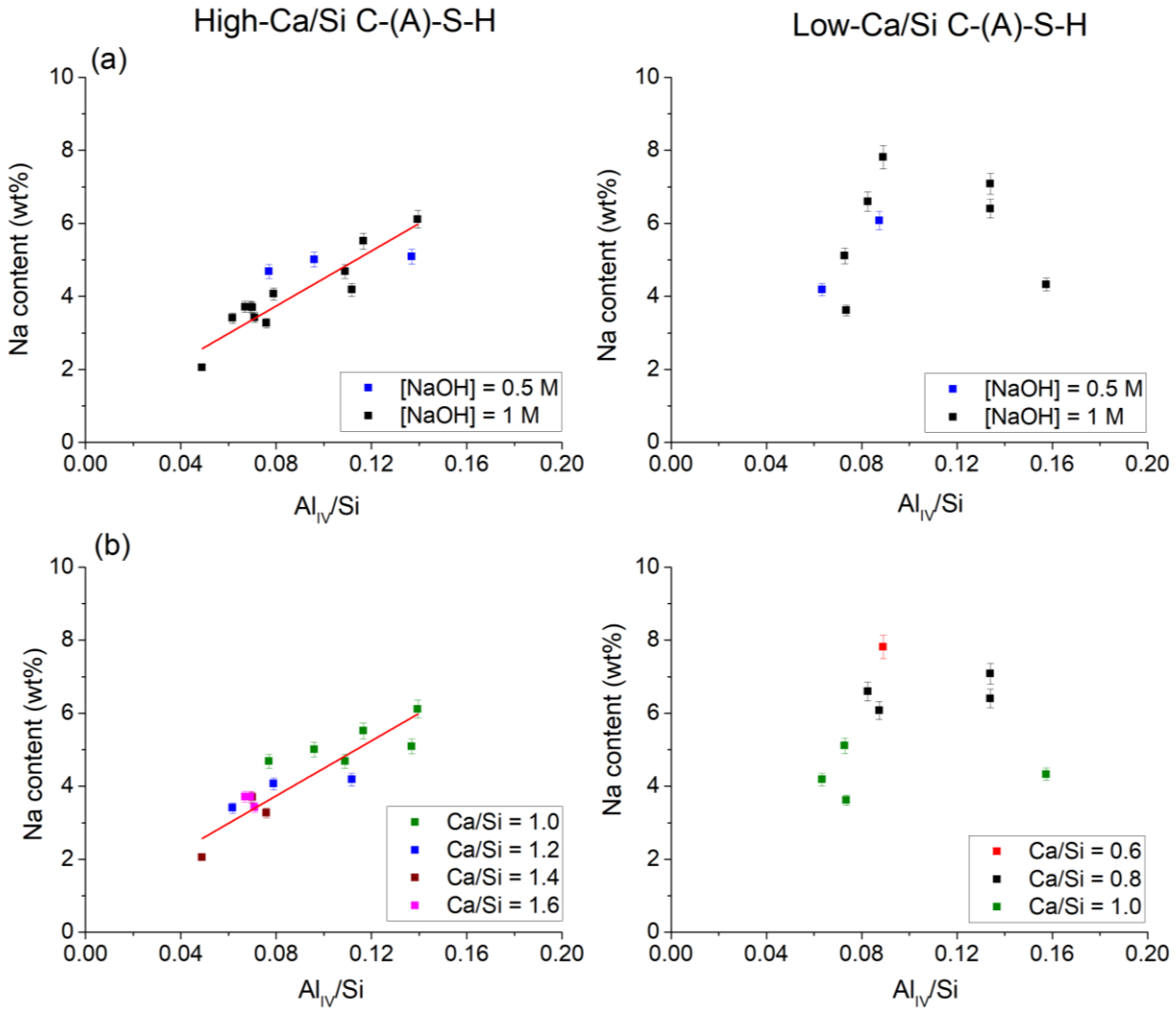

Figure 17. The Na contents in C-(A)-S-H samples from ^{23}Na NMR as function of the Al_{IV}/Si ratios determined by ^{27}Al NMR separated into two groups corresponding to average pure silicate chain lengths in the ranges 2.74 – 3.13 ($<\overline{CL}_{Si}> = 2.99$; high-Ca/Si C-(A)-S-H) and 3.73 – 6.00 ($<\overline{CL}_{Si}> = 4.79$; low-Ca/Si C-(A)-S-H). The graphs in part (a) highlight the dependencies of the NaOH solution concentration whereas part (b) discriminates between different Ca/Si ratios. The data are summarized in Tables S1 and S2.

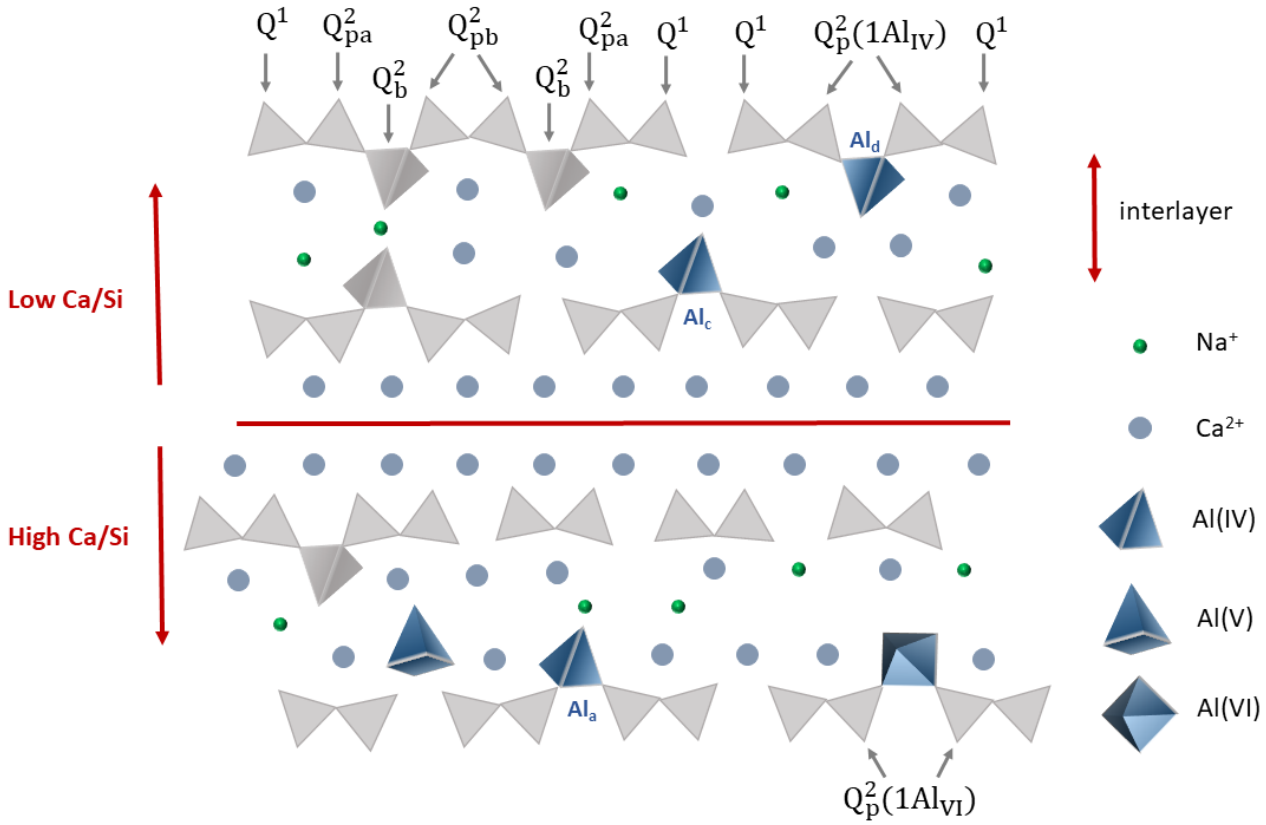

Figure 18. Schematic illustration of the proposed C-(A)-S-H structures with low and high Ca/Si ratios based on a defect-tobermorite model and the ^{23}Na, ^{27}Al and ^{29}Si NMR experiments conducted in this work. The proposed assignments for the different silicate sites and aluminum sites to the reported ^{29}Si (Table 1) and ^{27}Al (Table 6) chemical shifts are also given. Al_a(IV): charge-balanced by Na^+ and H^+; Al_c(IV): by ½Ca^{2+} ion and H^+; Al_d(IV): by Ca^{2+} ions or a combination of Ca^{2+} and Na^+ ions.

TOC Graphic

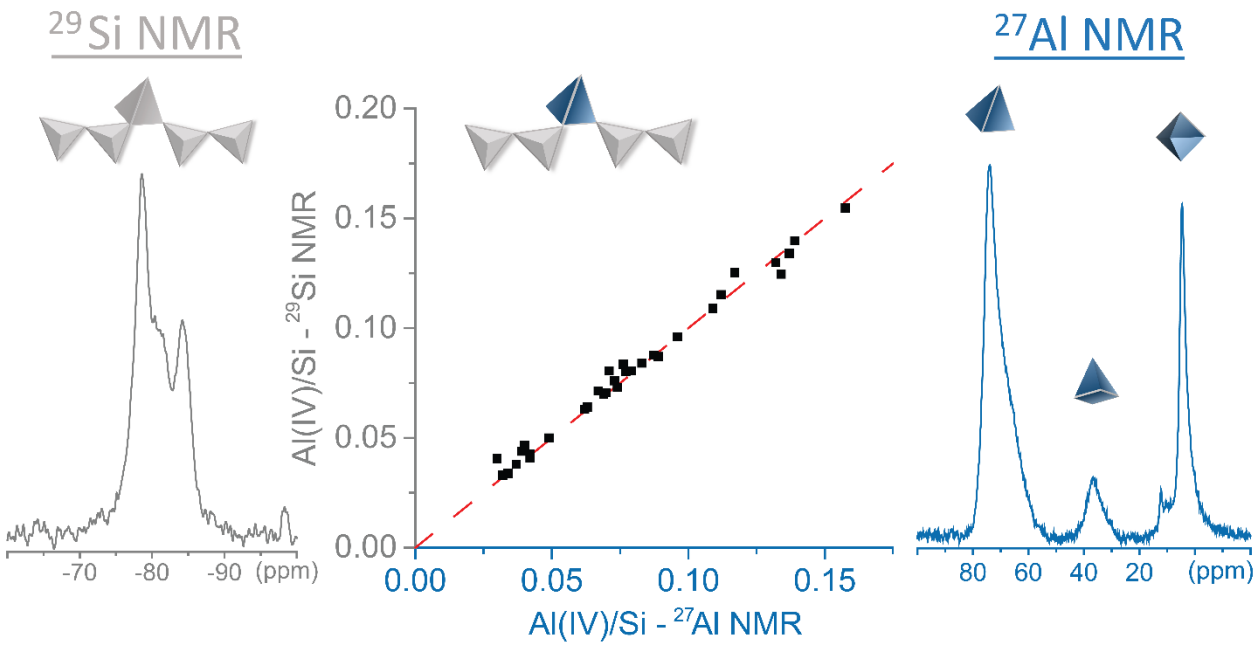
29Si NMR
-70
-80
-90
(ppm)
0.20
0.15
0.10
0.05
0.00
Al(IV)/Si - 29Si NMR
0.00
0.05
0.10
0.15
Al(IV)/Si - 27Al NMR
27Al NMR
80
60
40
20
(ppm)